Bioactive Materials 22 (2023) 291–311

Contents lists available at ScienceDirect

Bioactive Materials

journal homepage: www.keaipublishing.com/en/journals/bioactive-materials

Review article

Expedient secondary functions of flexible piezoelectrics for biomedical energy harvesting

Yuan Wang [a,**], Min Hong [b], Jeffrey Venezuela [a], Ting Liu [a], Matthew Dargusch [a,*]

[a] Centre for Advanced Materials Processing and Manufacturing (AMPAM), The University of Queensland, Brisbane, Queensland, 4072, Australia
[b] Centre for Future Materials, University of Southern Queensland, Springfield, Queensland, 4300, Australia

ARTICLE INFO

Keywords:
Flexible piezoelectrics
Stretchable
Hybrid energy harvesting
Self-healing

ABSTRACT

Flexible piezoelectrics realise the conversion between mechanical movements and electrical power by conformally attaching onto curvilinear surfaces, which are promising for energy harvesting of biomedical devices due to their sustainable body movements and/or deformations. Developing secondary functions of flexible piezoelectric energy harvesters is becoming increasingly significant in recent years via aiming at issues that cannot be addressed or mitigated by merely increasing piezoelectric efficiencies. These issues include loose interfacial contact and pucker generation by stretching, power shortage or instability induced by inadequate mechanical energy, and premature function degeneration or failure caused by fatigue fracture after cyclic deformations. Herein, the expedient secondary functions of flexible piezoelectrics to mitigate above issues are reviewed, including stretchability, hybrid energy harvesting, and self-healing. Efforts have been devoted to understanding the state-of-the-art strategies and their mechanisms of achieving secondary functions based on piezoelectric fundamentals. The link between structural characteristic and function performance is unravelled by providing insights into carefully selected progresses. The remaining challenges of developing secondary functions are proposed in the end with corresponding outlooks. The current work hopes to help and inspire future research in this promising field focusing on developing the secondary functions of flexible piezoelectric energy harvesters.

1. Introduction

The increasingly aging world's population has stimulated the development of patient-centred healthcare over the conventional hospital-centred diagnosis. The Internet of Things (IoT) technology provides a viable solution by ubiquitously employing trillions of smart devices, sensors, and actuators to realise real-time patient-centred monitoring/diagnosis [1]. Despite the miniaturisation of electronics and ultra-low power communication techniques, the regular replacement or recharging of power devices such as batteries and supercapacitors is still required, which not only increases the cost but might induce complications for long-term implantable electronics at hard-to-reach sites. Piezoelectrics can scavenge and harvest mechanical energy from the human body and in turn generate electrical power, therefore acting as stable, eco-friendly, and maintenance-free energy sources to power biomedical sensors or actuators [2,3]. In addition, biomedical piezoelectrics have the advantages including superior biocompatibility, facile processability, high durability, reliability, and sensitivity [4], therefore serving as a promising solution for biomedical energy harvesting. Fig. 1 (a) shows the past and the predicted global market of piezoelectric devices from 2017 to 2026 [5]. An enormous and steadily expanding market is witnessed, which is predicted to reach 27.5 billion US dollars in 2026. Particularly, lightweight flexible piezoelectric devices can conformally attach to curved human joints and organs, serving as biomedical sensors by harvesting mechanical energy. A flexible piezoelectric energy harvester typically contains a flexible piezoelectric thin film, as shown in Fig. 1(b). Two electrodes are attached on the top and bottom surfaces to form a sandwich like structure that is encapsulated by an outer flexible substrate. Fig. 1(c) exemplifies the wearable and implantable biomedical devices based on flexible piezoelectric energy harvesters [6–18]. These devices are found in diverse applications as energy generators or medical actuators, indicating the huge potential of flexible piezoelectrics in the biomedical field.

So far, flexible piezoelectric energy harvesters have been extensively

Peer review under responsibility of KeAi Communications Co., Ltd.
* Corresponding author.
** Corresponding author.
E-mail addresses: yuan.wang@uq.edu.au (Y. Wang), m.dargusch@uq.edu.au (M. Dargusch).

https://doi.org/10.1016/j.bioactmat.2022.10.003
Received 1 August 2022; Received in revised form 1 October 2022; Accepted 3 October 2022

reported to be fabricated from: (i) inorganic piezoelectric materials, including semiconducting nanowires (e.g., ZnO [3,20], GaN [21,22], CdS [23], InN [24], and ZnS [25]), lead-based (e.g., lead zirconate titanate (PZT) [26], $PbZrO_3$ [27], and PbTiO3 [28]) and lead-free ceramics thin films (e.g., BaTiO3 [29], LiNbO3 [30], $(K,Na)NbO_3$ (KNN) [31], and $LiTaO_3$ [32]); (ii) organic piezoelectric materials including synthetic polymers (e.g., poly(vinylidene fluoride) (PVDF) [33,34], poly (vinylidene fluoride-co-tri-fluoroethylene) (PVDF–TrFE) [35], nylon-11 (PA-11) [36], polylactic acid (PLA) [37], poly(L-lactide) (PLLA) [38], and poly(D-lactide) (PDLA) [39]), natural organics (e.g., amino acid [40], peptide [41], protein [42], and virus [43,44]), and molecular ferroelectrics [45]; and (iii) piezoelectric composites composing of conductive fillers (e.g., graphene [46], carbon nanotubes [47], and silver [48]), or non-conductive fillers (e.g., PZT [49], $BaTiO_3$ [50], KNN [51], ZnO [52], MgO [47], and TiO_2 [47]), and matrix (e.g., PVDF [49], P(VDF-TrFE) [47], hydroxyapatite [53], PDMS [51], and polyvinylidene fluoride hexafluoropropylene (PVDF-HFP) [46]). Numerous studies have been dedicated to significantly improve the output power of flexible piezoelectric devices via materials engineering (e.g., texture/crystallinity enhancement [54–57], dipole/polarisation alignment [41,58], doping engineering [59–61], surface micro-morphologies design [62–64], and nanocomposite [8,65,66]), and device design (e.g., Y-shaped attachment [67], operation mode adjustment [68], and gated-controlled piezotronics [69]). Reports on some impressive devices include a highly efficient PZT thin film nanogenerator that can light up 105 LEDs at the same time with an unbending motion [26], and a curved PVDF energy harvester able to light up 476 LEDs by a press-and-release motion [70].

Nevertheless, some issues that are irrelevant to output enhancement still hinder the practical applications of flexible piezoelectric devices. These issues include:

(i) Stretching-induced loose interfacial contact, user discomfort, and pucker generation due to soft and curvilinear body surfaces;
(ii) Power shortage or intermittency under working environments with inadequate mechanical energy;
(iii) Premature degeneration or failure of device function due to fatigue fracture generation after cyclic mechanical loading and unloading.

The proposed solution to the above issues revolves around developing specific secondary functions in flexible piezoelectrics, including stretchability, hybrid energy harvesting, and self-healing.

Previously, several reviews have been reported providing excellent overviews of flexible and stretchable piezoelectric energy harvesters [71–74]. However, a comprehensive and insightful review of multiple promising secondary functions of flexible piezoelectric energy harvesters that tackle issues irrelevant to improving piezoelectric output, including stretchability, hybrid energy harvesting, and self-healing, is still lacking. In this context, this review firstly introduced the fundamentals of piezoelectricity to provide a proper foundation for associated concepts and the development of secondary functions. Afterwards, backgrounds, mechanisms, and strategies to develop expedient secondary functions of stretchability, hybrid energy harvesting, and

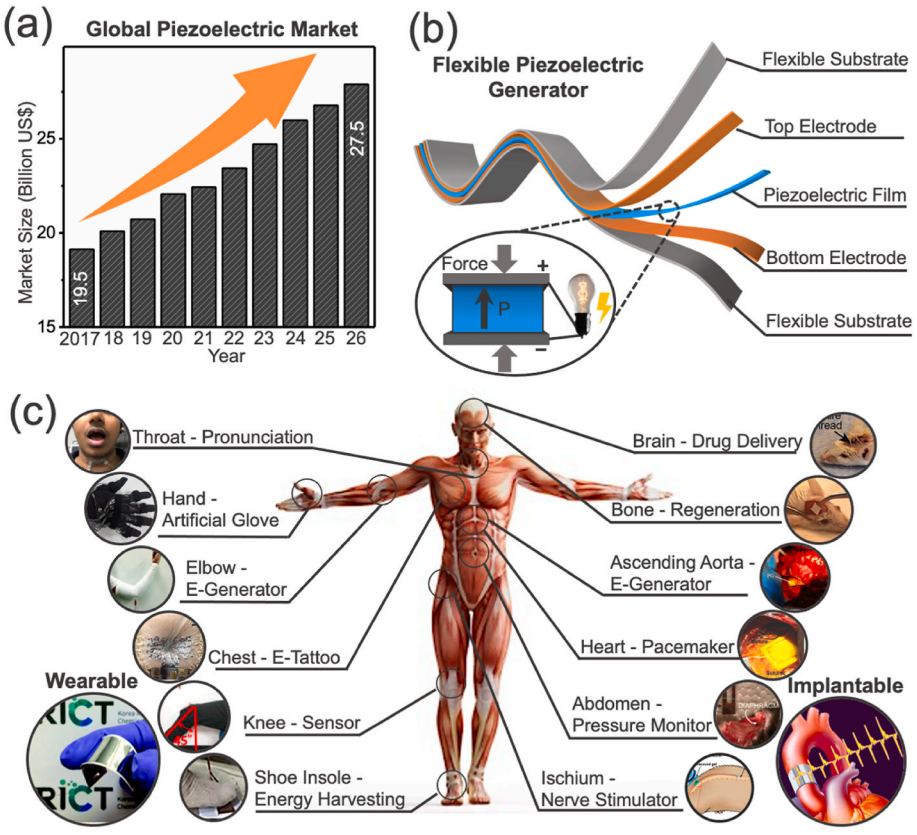

Fig. 1. Backgrounds of flexible piezoelectric devices for biomedical applications. (a) The past and the predicted global market sizes of piezoelectric devices from 2017 to 2026 [5]. (b) The typical structure of flexible piezoelectric devices. (c) The diverse biomedical applications of flexible piezoelectric devices as wearable electronics (Reproduced with permission [8]. Copyright 2018, Royal Society of Chemistry), including pronunciation monitor [6] (Reproduced with permission [6]. Copyright 2017, American Chemical Society), artificial glove [7] (Reproduced with permission [7]. Copyright 2017, Institute of Physics), electricity generator [8] (Reproduced with permission [8]. Copyright 2018, Royal Society of Chemistry), e-tattoo [9] (Reproduced under the terms of the CC-BY Creative Commons Attribution 4.0 International license (https://creativecommons.org/licenses/by/4.0) [9]. Copyright 2019, The Authors, published by Wiley-VCH), movement sensor [10] (Reproduced with permission [10]. Copyright 2015, Elsevier), and energy harvesting shoe insole [11] (Reproduced with permission [11]. Copyright 2020, American Chemical Society); as implantable devices (Reproduced with permission [14]. Copyright 2015, Elsevier), including blood–brain barrier opener [12] (Reproduced under the terms of the CC-BY Creative Commons Attribution 4.0 International license (https://creativecommons.org/licenses/by/4.0) [12]. Copyright 2020, The Authors, published by United States National Academy of Sciences), bone tissue stimulator [13] (Reproduced with permission [13]. Copyright 2020, Elsevier), aorta electricity generator [14] (Reproduced with permission [14]. Copyright 2015, Elsevier), pacemaker [15] (Reproduced with permission [15]. Copyright 2021, Elsevier), abdomen pressure monitor [16] (Reproduced under the terms of the CC-BY Creative Commons Attribution 4.0 International license (https://creativecommons.org/licenses/by/4.0) [16]. Copyright 2018, The Authors, published by United States National Academy of Sciences), and neural stimulator [19] (Reproduced under the terms of the CC-BY Creative Commons Attribution 4.0 International license (https://creativecommons.org/licenses/by/4.0) [19]. Copyright 2020, The Authors, published by Springer Nature).

self-healing are respectively discussed by reviewing carefully selected progresses. In the end, the remaining challenges of the above secondary functions are respectively proposed with corresponding future outlooks. This paper hopes to provide a reference and inspire future research in this promising field focusing on developing the secondary functions of flexible piezoelectrics, which is of vital significance to advance their biomedical applications.

It should be noted that the commercialisation of biomedical piezoelectric energy generators should also consider their narrow bandwidth, and the scalable manufacturing of not only piezoelectric energy harvester but also its integrated circuit and energy storage device, as well as encapsulation. In addition, biomedical energy harvesters, especially bio-implantable energy harvesters, are required to be biocompatible, which necessitates biocompatible device components including piezoelectric material, electrode, substrate, and encapsulation [75]. For piezoelectric biomedical energy harvesters, electrode materials have been reported including Cr [76], Ag [77], Cu [78], Au [76], Al [79], graphene [80], and indium tin oxide (ITO) [81], substrate materials have been reported including plastic films (e.g., polyethylene terephthalate (PET) [82,83], and polyimide(PI) [84]) and metallic foils (e.g., Ni [85], Pt [86], and Ni–Cr alloy [87]), and encapsulation materials have been reported such as PI [84], PDMS [88], and PDMS/Parylene-C [89]. Initial studies have confirmed their biosafety [76,89], but long-term biocompatibility studies using large animal models or clinical studies are highly desired to conclude on their long-term biocompatibility. In terms of piezoelectric material, high-performance lead-free piezoelectric ceramics [90,91] and piezoelectric polymers [2] have been widely reported to be biocompatible, while lead-based ceramics may also be biocompatible in the crystalline state [92] or under proper encapsulation [84]. However, for bio-implantable energy harvesters, only lead-free piezoelectric ceramics and polymers are expected to be utilised, considering the wet and complex physiological environment-induced varying degrees of solubility and potential ion penetration/leakage, especially for long-term implantation applications.

2. Fundamentals of piezoelectricity in brief

The word “piezo” is a Greek word meaning “to press”, therefore piezoelectricity logically and appropriately depicts the generation of electricity by pressing. Piezoelectricity was firstly discovered by French physicist Pierre Curie and his older brother Jacques Curie in 1880 [93]. They found that mechanical stress can induce the production of surface charges in a range of crystals, such as tourmaline, quartz, and topaz. Subsequently, the converse piezoelectric effect, i.e., the generation of mechanical strain induced by electricity, was thermodynamically predicted by Franco-Luxembourgish physicist Gabriel Lippmann in 1881 [94], and later experimentally confirmed by the Curie brothers. Since then, investigations on understanding fundamentals and discovering applications of piezoelectricity have been exponentially grown [95–97].

2.1. Piezoelectricity mechanisms

The mechanisms of piezoelectricity are separately introduced for inorganic and organic piezoelectric materials. For inorganic piezoelectric materials, piezoelectricity requires a non-centrosymmetric crystal structure [2], or the symmetry breaking of some inorganic materials such as hydroxyapatite [98]. The piezoelectric voltage is engendered by a net mechanically induced polarisation in the crystal. Specifically, when mechanical strain is applied, the atomic structure is deformed and thus induces the displacement of ion balance, as exemplified in Fig. 2(a) for the case of PZT. The shift of ion balance leads to the formation of a dipole moment in the crystal unit. Adjoining dipoles tend to be aligned, forming a Weiss domain with a net dipole density or polarisation. Polarisation directions are random in the crystal. To form a net

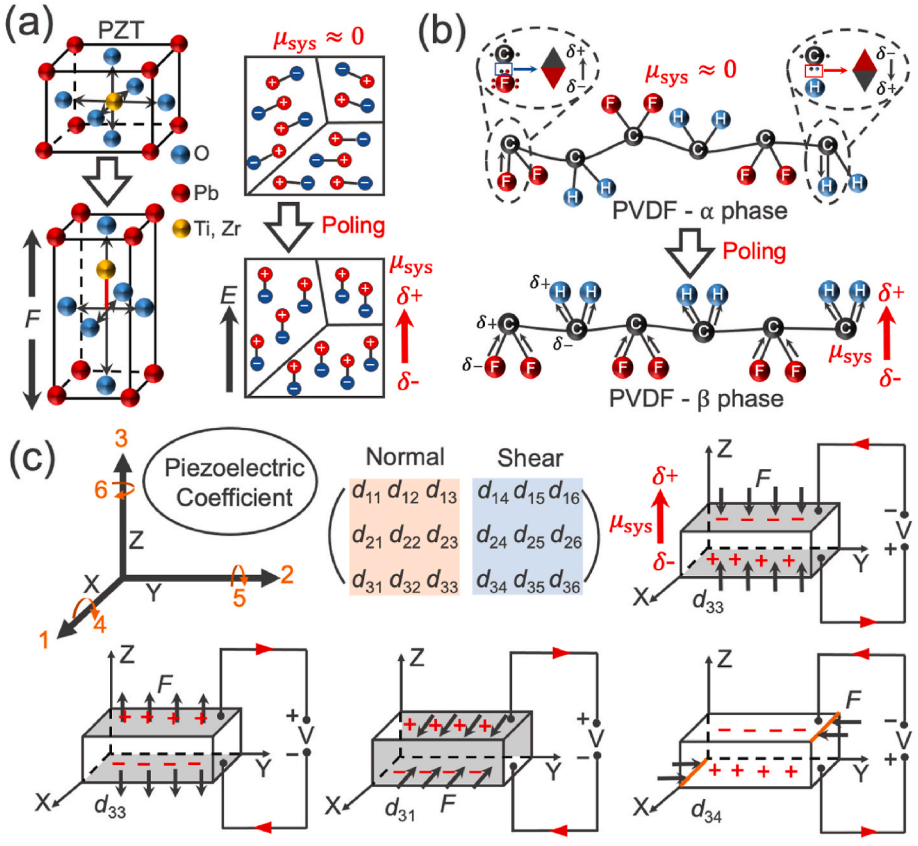

Fig. 2. Piezoelectricity fundamentals. The piezoelectricity mechanisms of (a) inorganic PZT and (b) organic PVDF piezoelectric materials. (c) The three-axis coordinate system of piezoelectric directions and piezoelectric charge coefficient diagrams.

polarisation in the crystal upon mechanical stress, inorganic piezoelectric materials need to be poled under a high electric field at an elevated temperature to regulate polarisation along the direction of the poling electric field, as shown in Fig. 2(a). As a result, a net polarisation can be generated in the crystal under proper mechanical stress, leading to piezoelectric charges on the surface of inorganic piezoelectric materials. Conversely, piezoelectric materials can generate mechanical deformations by applying external electric fields, called the converse piezoelectric effect.

The piezoelectricity of organic piezoelectric materials can be understood as the reorientation of molecular dipoles induced by an intense electrical field or mechanical stretching [99]. Fig. 2(b) exemplifies the piezoelectricity mechanism of PVDF [100]. The different electronegativities between atoms, i.e., carbon-fluorine and carbon-hydrogen, lead to the formation of randomly distributed molecular dipoles in PVDF, pointing from negative (high electronegativity) to positive (low electronegativity) charges. For the α phase in PVDF, the molecular dipoles are antiparallel, therefore the net dipole is close to zero and PVDF is unpolarised. By poling PVDF with a high electrical field and stretching, α phase can be transformed into β phase where molecular dipoles become mostly parallel, resulting in a polarised PVDF.

2.2. Piezoelectric coefficients

Piezoelectric coefficients depict the relationships between piezoelectric responses and the directions of applied external stimuli. Various piezoelectric coefficients can be used to depict the piezoelectric responses of interest, including the charge coefficient (d, the response of polarisation charge, C N^{-1}; or the response of strain, m V^{-1}), the voltage coefficient (g, the response of electric field, V m N^{-1}), the permittivity coefficient (ε, the response of dielectric displacement, farad m^{-1}), and electromechanical coupling coefficient (k, the response of electromechanical coupling, dimensionless).

Considering the anisotropy of piezoelectric materials, the identification of directions in a piezoelectric element is important to characterise piezoelectric responses. Therefore, a three-axis coordinate system is utilised to define piezoelectric directions, as shown in Fig. 2(c). The three directions X, Y and Z in the classic orthogonal coordinate system are defined as the directions 1, 2 and 3 for the normal piezoelectricity, while their shear directions are defined as the directions 4, 5 and 6 for the shear piezoelectricity, respectively. On this basis, directions of piezoelectric coefficients can be described using two subscripts, i and j, where i represents the direction of generated electrical field or applied voltage, while j reflects the direction of applied mechanical stress or induced strain. Fig. 2(c) exemplifies the diagrams of d_{33}, d_{31} and d_{34}, where the poling direction is considered as the "3" direction. As can be seen, surface charges and therefore electric fields can be generated in the "3" direction by mechanically deforming piezoelectric materials along the "3" (d_{33}) or the "1" direction (d_{31}) or applying shear stresses along the "4" direction (d_{34}). By reversing the direction of deformation, for example, by applying mechanical tension rather than compression, an opposite electric field can be generated, as exemplified in the d_{33} diagrams.

In addition to the subscripts, superscripts are also applied to further specify their mechanical or electrical boundary conditions of piezoelectric coefficients. For example, $\varepsilon_{ij}^{T}$is the permittivity under a constant stress field. In this way, the piezoelectric effect and the converse piezoelectric effect can be described using the following two equations [101], respectively:

$$D = d \bullet T + \varepsilon^{T} E \text{ (direct effect)} \quad \text{(Eq. 2.1)}$$

$$S = s^{E} \bullet T + d^{t} \bullet E \text{ (converse effect)} \quad \text{(Eq. 2.2)}$$

where D and E are respectively the electric displacements and electric field vectors, S and T are the strain and stress tensors, respectively, s^{E} is the elastic compliance matrix under a constant electric field, while d and d^{t} are the coefficient matrices for the piezoelectric effect and the converse piezoelectric effect (d^{t} is the transposition of d), respectively. Piezoelectricity therefore can be essentially understood as the generations of electric charges (D) or strains (S) by applying mechanical stress (T) and/or electric field (E), whose behaviours are unique to the direction and depend upon material-intrinsic parameters (d, ε and s).

Based on above fundamentals, considerations are required when developing secondary functions to prevent undesirable function interference or counteraction. Firstly, since piezoelectric outputs are direction-dependent, structure manipulation, such as developing 3D stretchable structures, needs to be coupled with mechanics analysis (e.g., finite element analysis) to guide external forces preferentially loaded in directions with strong piezoelectric responses to prevent significant output deterioration. Secondly, microstructure engineering, such as engineering dynamic hydrogen bond networks and proton interactions for self-healing capacity, needs to consider the impact on material crystallinity or chain arrangement, which may lead to the counteraction of local dipole moments and degenerated piezoelectric performance. Thirdly, a portion of piezoelectric materials is also pyroelectric materials, whose dipole moments can be thermally induced to generate pyroelectric voltage and vice versa. Proper thermal management is necessary when developing hybrid energy harvesters to avoid unexpected conflicts between various energy harvesting systems.

3. Stretchability

Due to the soft and curvilinear surfaces of human limbs, joints, and organs, the practical applications of flexible piezoelectrics suffer from issues including user discomfort, loose interfacial contact, poor wrinkle resistance, and pucker or even breakage. To this end, developing stretchable flexible piezoelectrics is necessary, which affords the capacity to eliminate above issues by conformally attaching onto curvilinear and soft surfaces during stretching. It will also lead to smaller device size and greater design flexibility. The increase in allowable strain enabled by stretchability may also contribute to improved piezoelectric output and sensitivity.

Basically, the stretchability of flexible piezoelectrics can stem from four classes of strategies, including (i) nano/micro-structure design, (ii) morphology design, (iii) elastic piezoelectric or non-piezoelectric matrix, and (iv) stretchable interconnections and substrates for devices based on rigid piezoelectric arrays. In this section, state-of-the-art strategies to develop stretchable flexible piezoelectrics are classified based on the above criteria and discussed by understanding structural characteristics and material properties. The evolution of each class of strategies is reflected by highlighting the improved aspect of evolved strategies compared with earlier ones. The impacts of stretchability on piezoelectric behaviour are also discussed.

3.1. Microstructure design

Designing stretchable microstructures has been proven as an effective strategy to induce stretchability. Fig. 3(a) shows a wavy microstructure of PZT ribbons [102], formed by releasing pre-strained flat PZT ribbons (buckling process) [103]. The buckled PZT ribbons possess a wavy microstructure along the out-of-plane direction, enabling the crack-free tensile strain. The increased stretchability is attributed to the accommodation of in-plane deformations enabled by wavy microstructure by varying its wavelength and amplitude. The wavy microstructure also leads to significantly higher piezoelectric current density, for example, 250 μA cm^{-2} [102] than 4 μA cm^{-2} of non-stretchable PZT nanowires-based energy generator [104], due to the much higher strain gradients at buckled regions than flat regions and also the absence of the substrate clamping effect [105]. On top of which, Su et al. further stacked wavy microstructured PZT ribbons into a multilayered architecture for increased piezoelectric output, by which the peak voltage can

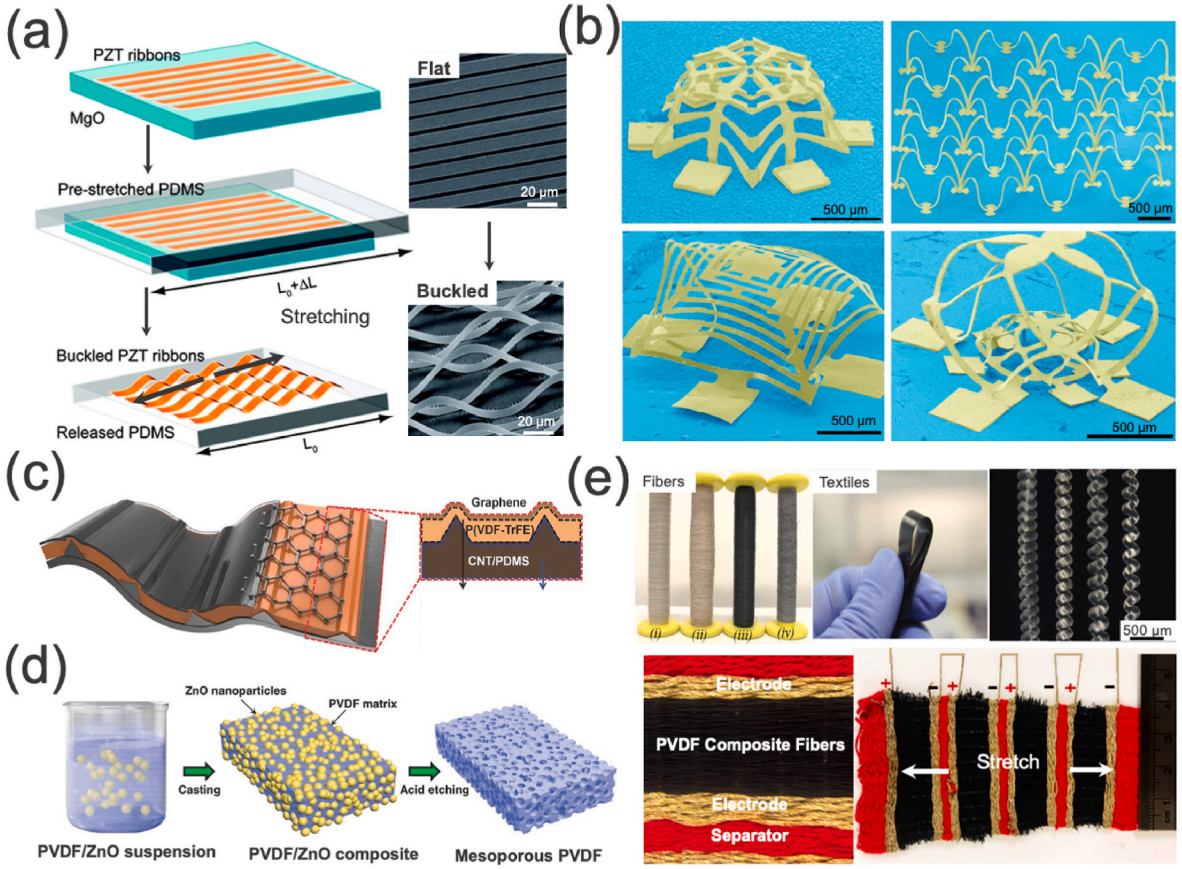

Fig. 3. Microstructure design of stretchable flexible piezoelectrics. Stretchable microstructures including (a) buckled microstructure [102], (b) complex 3D microstructure [109], (c) wavy interfacial pattern [115], (d) microporosity [116], and (e) coiled microstructures [117]. (a) Reproduced with permission [102]. Copyright 2011, American Chemical Society. (b) Reproduced with permission [109]. Copyright 2019, Springer Nature. (c) Reproduced with permission [115]. Copyright 2013, Wiley-VCH. (d) Reproduced with permission [116]. Copyright 2014, Wiley-VCH. (e) Reproduced under the terms of the CC-BY Creative Commons Attribution 4.0 International license (https://creativecommons.org/licenses/by/4.0) [117]. Copyright 2020, The Authors, published by Wiley-VCH.

increase from 3.7 V (single PZT ribbon) to 8.1 V by stacking 5 PZT ribbons [106]. The operation modes of stretchable wavy piezoelectric ribbons are limited by their simple geometries. Developing deterministic complex 3D microstructures [107] can extend their operation modes and provide the desired stretchability. It has been found that the motions of ribbons are dominated by out-of-plane bending and twisting deformations, and the bending and torsional degrees of freedom of ribbons are constrained by deformations' isometric nature (i.e., length invariant) [108]. By compressively buckling delicately designed 2D patterns, sophisticated 3D microstructures can be fabricated to enable a notably wider frequency range of vibrations and larger piezoelectric output than 2D serpentine, as shown in Fig. 3(b) [109].

Above out-of-plane wavy microstructure may suffer from thick encapsulation and poor pressing-mode (d_{33}) piezoelectric responses [110]. An in-plane wavy microstructure may prevent the above drawbacks while maintaining the desired stretchability. This was reported from stretchable PVDF nanoribbons [111,112], which was fabricated by printing straight PVDF nanofibers onto pre-strained PDMS substrate followed by releasing. The pre-strain and the space among printed nanofibers were simulated and designed to realise large scale in-plane wavy fibres with high uniformity and integration, which contribute to a much higher in-plane strain of 110% [111]. This strategy was later optimised by printing fractal PVDF nanofibers [113], i.e., a structure with a higher buckle density, combined with liquid metal interconnection electrodes. Consequently, an improved stretchability of 200% was achieved by Huang et al. [113]. By designing the pre-strain of PVDF nanofibers and optimising printing parameters, the same group later realised wavy serpentine PVDF nanofibers with a further improved stretchability of 300% [114].

Fig. 3(c) demonstrates a stretchable P(VDF-TrFE) film on a micropatterned carbon nanotube (CNT)-PDMS electrode [115]. The stretchability was attributed to the wavy interfacial pattern between the film and electrode, which enables a strain of 30% without cracking [115]. Siddiqui et al. [80] applied the similar micro-pattering strategy but using stacked $BaTiO_3$–P(VDF-TrFE) composite mats. Due to the stress-relieving effect induced by micropattern and the free-standing nature of stacked mats, increased stretchability of 40% was achieved with a peak open-circuit voltage of 10.1 V.

In addition, microporosity has been reported to enhance the stretchability of PVDF films [116], as shown in Fig. 3(c). Compared with rigid plastic films under low porosity, it was found high porosity (>40%) can lead to sponge-like soft and lossy PVDF films, yielding a considerably larger displacement and higher electrical output under the same external impact.

Overtwisting can produce stretchable microstructures for piezoelectric fibres [117–119]. A very high strain of 740% has been reported by twisting PVDF-TrFE nanofibers into yarns and then overtwisting yarns into a stretchable coiled structure [118]. The high stretchability was ascribed to the interaction forces between nanofibers, including friction, van der Waals, and electrostatic forces. To further enhance the output of piezoelectric fibres, polar phase stabilising fillers can be incorporated to develop composite fibres [120]. Mokhtari et al. [117] developed PVDF/$BaTiO_3$/reduced graphene oxide (rGO) composite fibres with a coiled structure to fabricate a stretchable piezoelectric textile, as shown in Fig. 3(c). $BaTiO_3$ nanoparticles present high dipole attractions and can stabilise the electroactive β-phase by electrostatic

interactions and hydrogen bonding with PVDF chains, while conductive rGO particles can provide free electronic charges to promote the formation of PVDF/$BaTiO_3$ dipoles in the composite. The textile device generated a high voltage output of 1.2 V and presented a high strain of 100%. Despite the high stretchability, coiled stretchable fibres might suffer from poor piezoelectric regularity, especially under high strains, because the deformation tends to occur by micro-buckle unfolding rather than coil opening.

3.2. Morphology design

Stretchable morphologies have been reported including textile, filamentary serpentine (FS), and the kirigami structures.

Fig. 4(a) shows a typical stretchable textile based on piezoelectric PVDF threads [121]. Such a structure is fabricated by weaving silicon tube column threads with PVDF row threads into stitches. When the structure is stretched, PVDF threads undergo tensile stresses, while the alternately patterned elastic polyester patches on PVDF threads contribute to the thread contraction, generating piezoelectric voltages during continuous stretches and contractions. Based on that, Ahn et al. further used piezoelectric column straps weaved with piezoelectric row straps, separated by elastic hollow tubes [122]. In addition to enhanced piezoelectric output, as-fabricated stretchable textile can also serve as a tactile sensor, due to the distance change and thus the capacitance change between column and row threads enabled by the hollow tubes during stretching and compressing. Kim et al. reported a helical structure which might be used to significantly improve the stretchability of aforementioned piezoelectric thread/strap [123]. As shown in Fig. 4(b), the helical structure was formed by twinning PVDF strap and fabric band around an elastic core in the opposite direction, which enabled a high stretchability up to 158%. By stitching the helical piezoelectric harvester with clothes, piezoelectric voltages of 3.9 and 4.4 V can be generated during push-up and squatting motions, respectively. Above stretchable textiles may suffer from electrical shorting under wet environments. This can be prevented by introducing cotton threads as the insulating spacer between electrodes [124], or developing a core-shell structure where the inner electrode is fully shield and isolated from the outer electrode consisting of conductive yarn [125,126].

The stretchable FS structure [9,127] is depicted in Fig. 4(c), which was applied to fabricate a PVDF-based piezoelectric e-tattoo for mechano-acoustic cardiovascular sensing [9]. The fabrication was realised by a cut-and-paste process, where the FS-structured PVDF was firstly patterned by a mechanical cutter plotter, whose pattern was subsequently pasted by Au electrodes on the top. The FS e-tattoo presents a good stretchability of 100% and compatible deformations with human skin. However, the serpentine pattern in the FS structure is stress-relieving, which compromises the piezoelectric output and sensitivity. The sensitivity after stress-relieving (0.4 mV per micro-strain) is only 3.6% of that in stretching straight PVDF ribbons [9].

The undesirable output degradation induced by stress-relieving can be mitigated by kirigami structures, which can achieve stretchability by creating out-of-plane deformations above 2D flat sheets and realising complex 3D geometries. The stretchability of kirigami structures has been witnessed in lithium-ion batteries [128], cellular metamaterials [129], solar tracking system [130], etc. Its application in piezoelectrics was reported in 2018, when Hu et al. [131] found that kirigami PVDF films exhibited 18% strain without fracture while generating a slightly degraded piezoelectric output of 132 mV, in contrast to the 160 mV output observed in uncut PVDF films under a 1% strain. By rationally designing kirigami parameters such as cut density and cut position [131], the stress aggregation at the sharp corners of cuts, which can limit

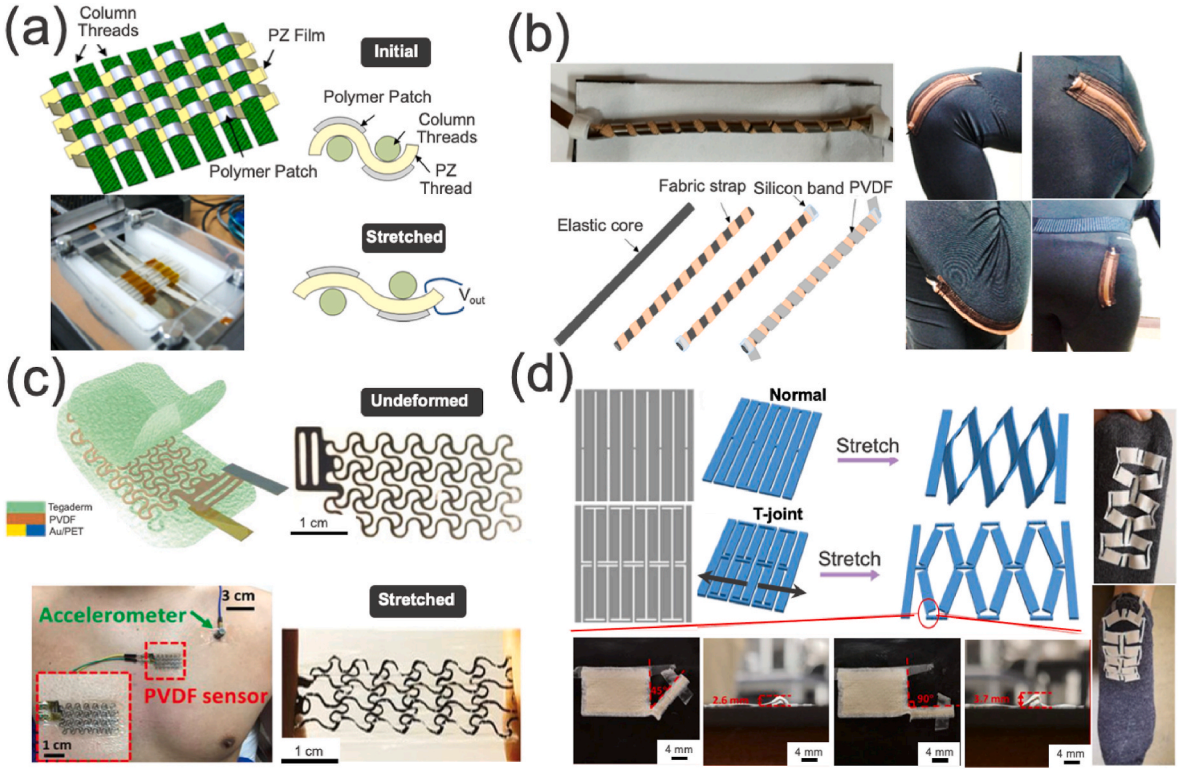

Fig. 4. Morphology design of stretchable flexible piezoelectrics. Stretchable morphologies including (a) textile [121], (b) helical strap [123], (c) filamentary serpentine (FS) meshing [9], and (d) kirigami cutting [110]. (a) Reproduced with permission [121]. Copyright 2013, Wiley-VCH. (b) Reproduced under the terms of the CC-BY Creative Commons Attribution 4.0 International license (https://creativecommons.org/licenses/by/4.0) [123]. Copyright 2017, The Authors, published by Multidisciplinary Digital Publishing Institute. (c) Reproduced under the terms of the CC-BY Creative Commons Attribution 4.0 International license (https://creativecommons.org/licenses/by/4.0) [9]. Copyright 2019, The Authors, published by Wiley-VCH. (d) Reproduced with permission [110]. Copyright 2020, Elsevier.

stretchability, can be minimised and thus realising improved piezoelectric outputs and stretchability. Sun et al. [132] utilised finite element analysis (FEA) simulations and found that the conventional continuous electrode connection can lead to charge cancellation from opposite strains on the electrode, thereby deteriorating piezoelectric outputs. They reported a segmented electrode connection to address this issue, where electrodes were deposited only at regions of the highest strain. The output voltage of the kirigami-structured sensor was consequetly improved by 2.6 times and reached 1.63 V under a tensile strain of 10% [132]. The piezoelectric performance of kirigami structure can be further improved by controlling the cut shape, so that the optimal piezoelectric mode can be adopted [110]. Specifically, simple kirigami structures typically function by the out-of-plane tilting during stretching, which disables the most facile and common "3-3" mode to harvest energy by pressing. A T-joint-cut, as shown in Fig. 4(d), can overcome this issue by introducing a joint point to connect short and long cuttings, so that the out-of-plane tilting occurs only at the joint point during stretching, and other places are flat to enable "3-3" mode to harvest energy by pressing. The joint point also enables the rotation of other parts around during stretching, which leads to enhanced stretchability. As a result, the kirigami-structured sensor with a T-joint-cut presented an impressive strain of 300% with an open current voltage of 6 V [110].

3.3. Elastic matrix and stretchable interconnections

For piezoelectric composites [133], both piezoelectric polymers and non-piezoelectric elastomers have been reported to contribute to stretchability as the elastic matrix. PVDF [79,134] and its copolymers such as P(VDF-TrFE) [135,136] and PVDF-HFP [137] are mostly used piezoelectric polymers, while PDMS [6,138] and silicone elastomer [77,139,140] are commonly applied as the elastomer.

Studies on piezoelectric polymer-based stretchable composites have been devoted to improving their piezoelectric output and mechanical properties. Among which, incorporating engineered fillers such as doped ZnO [137,141], surface charged Al_2O_3 [142], Ag nanoparticles [143,144], SnO_2 nanosheet [145], and graphene [146] has been proven as an effective strategy to increase the composite's energy output, and potentially improve its mechanical properties. The reason for the enhanced output can be essentially attributed to the interaction between fillers and polymer matrix, by which the content of polymer's main electroactive phase can be improved for stronger piezoelectric responses. For example, the positive surface charges of Co-doped ZnO nanofillers were reported to interact with the molecular dipoles (CH_2 or CF_2) of PVDF-HFP to improve its β-phase content [137,147], while the incorporation of graphene filler can achieve similar benefit by forming micro-capacitors in PVDF and improving polarisation efficiency and orientation of dipole moments due to its good dielectric properties [146,148]. Fig. 5(a) shows the mechanism of increased β-phase in PVDF-HFP induced by surface-charged Al_2O_3 nanoparticles [142]. When Al_2O_3 nano-fillers are dispersed in the matrix, their high surface energy and positive surficial charges induce the Coulomb repulsion among fillers and thereby ensure uniform filler distribution. Meanwhile, the

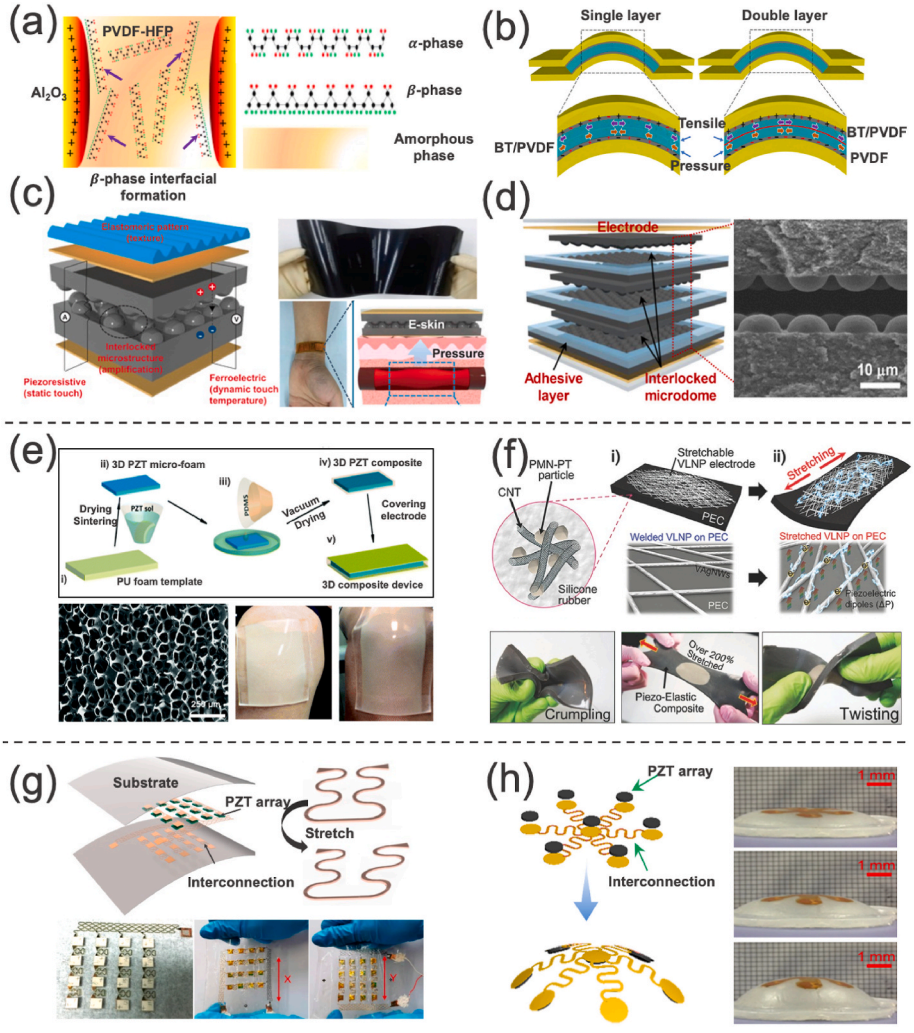

Fig. 5. Elastic matrix and stretchable interconnection of stretchable flexible piezoelectrics. Piezoelectric polymer-based elastic matrix with (a) surface charged Al_2O_3 fillers [142], (b) double-layered structure [150], (c) fingertip skin-like interlocked structure [64], and (d) multi-layered interlocked structure [164]. Non-piezoelectric elastomer-based elastic matrix with (e) PZT ceramic foam [169], and (f) multi-walled carbon nanotubes as physical distribution disperser [77]. Stretchable (g) serpentine structured Cu interconnections [170], and (h) claw-shape interconnections [171]. (a) Reproduced with permission [142]. Copyright 2019, Wiley-VCH. (b) Reproduced with permission [150]. Copyright 2018, Elsevier. (c) Reproduced under the terms of the CC-BY Creative Commons Attribution 4.0 International license (https://creativecommons.org/licenses/by/4.0) [64]. Copyright 2015, American Association for the Advancement of Science. (d) Reproduced with permission [164]. Copyright 2018, American Chemical Society. (e) Reproduced with permission [169]. Copyright 2018, Royal Society of Chemistry. (f) Reproduced with permission [77]. Copyright 2015, Wiley-VCH. (g) Reproduced with permission [170]. Copyright 2015, Wiley-VCH. (g) Reproduced under the terms of the CC-BY Creative Commons Attribution 4.0 International license (https://creativecommons.org/licenses/by/4.0) [170]. Copyright 2019, The Authors, published by Multidisciplinary Digital Publishing Institute. (h) Reproduced under the terms of the CC-BY Creative Commons Attribution 4.0 International license (https://creativecommons.org/licenses/by/4.0) [171]. Copyright 2021, The Authors, published by American Association for the Advancement of Science.

interfacial hydrogen bonding between charged filler surface and matrix orders PVDF-HFP chains to transform into crystallised β-phase, leading to a 5.6 times higher dielectric constant than pure PVDF-HFP polymer. On the other hand, the reason for filler incorporation to enhance the composite's mechanical properties may lie in the uniform filler distribution which can facilitate load transfer between filler-matrix interface [149]. Zhang et al. [79] reported eleven times and twice increase in the strength and stretchability of PVDF, respectively, after introducing uniformly distributed boron nitride nanosheets.

Structure engineering can also enhance the output of piezoelectric polymer-based stretchable composites. Fig. 5(b) shows a double-layered PVDF-based composite with barium titanate fillers embedded in the top PVDF layer and a pure PVDF layer at the bottom [150]. As shown, compared with single-layered structure which may degenerate piezo-response due to the counteraction of top and bottom opposite charges, the counteracting effect in double-layered structure is weak, and the additional charges accumulated at the heterointerface can induce higher composite's electric capacity. This structure can be further optimised by developing multi-layered piezoelectric composites [151,152], which can suppress the charge injection and migration at dielectric/electrode and dielectric/dielectric interfaces to significantly improve the breakdown strength and the charge density. Li et al. [153] investigated the influence of the number of layers on device performance and found that layer number higher than four will lead to an increased possibility of current leakage and piezoelectric electron-hole recombination, and overall deteriorated output performance. The optimal four-layered $BaTiO_3$/PVDF film generated promising piezoelectric voltage and current of 14.22 V and 2.42 A, respectively [153].

Micro-patterning and nano-templating [154] may also enhance the output of piezoelectric polymers using methods including electron/ion beam writing [155], layer-by-layer assembly [156], nanoimprinting [157], soft lithography [158], and patterned electrohydrodynamic pulling [159]. Surmenev et al. [160,161] found imprinted PVDF micropillars possessed 1.85 times stronger piezoelectric response than flat PVDF film counterparts, from 40 to 74 p.m. V^{-1}. This is because of the strain confinement effect of micropillars which can withstand a high strain upon applied loading. On the other hand, nano-templating using anodized aluminium oxide (AAO) template was found to possess a template confinement effect towards the alignment of polymer chain which can promote α-to-β phase transition in PVDF [162,163]. Fig. 5(c) [64], and **(d)** [164] show another novel micro-pattern inspired by fingertip skin. Compared with planar films, the interlocked micro-dome arrays possess a larger contact area and stress concentration effect between micro-domes, which can induce enhanced deformations and thus higher piezo-responses. Lee et al. [164] further increased the contact area by fabricating multi-layered e-skin with interlocked micro-dome arrays (Fig. 5(d)) and realised a high sensitivity of 47.7 kPa^{-1} with 1.3 Pa minimum detection.

Lastly, the output of ferroelectric and piezoelectric polymers may be significantly improved based on the cutting-edge discovery of the morphotropic phase boundary (MPB) [165] and the chirality-induced relaxor property [166] in P(VDF-TrFE). MPB used to be exclusive in the field of ferroelectric ceramics, whose composition enables the coexist of two or more competing phases (i.e., relaxor phase and normal ferroelectric phases), leading to more thermally dynamic ferroelectric dipoles, more facile polarisation reorientation, and therefore higher piezoelectric response [166,167]. The discovery of MPB in ferroelectric P(VDF-TrFE), and the origin of relaxor behaviours, provided the necessary fundamental knowledge to understand relaxor ferroelectric polymers and their composition design. Based on that, Park et al. [168] reported greatly improved piezoelectric voltage of 20 V and current of 210 nA from poled ferroelectric P(VDF-TrFE) nanofibers with 50% molar fraction of TrFE, compared with the 9.5 V and 110 nA obtained from normal poled P(VDF-TrFE) nanofibers with 30% molar fraction of TrFE. Such work may inspire future work to develop novel relaxor ferroelectric polymers serving as the promising matrix of high-performance stretchable piezoelectric composites.

In terms of non-piezoelectric elastomer-based stretchable composites, piezoelectric particles are dispersed in the matrix as fillers. Nevertheless, they may suffer from issues of (i) low piezoelectric output due to decreased content of effective piezoelectric materials and filler aggregation, (ii) unexpected fatigue failures due to poor filler dispersion in polymer matrix with high viscosity, and (iii) poor connection among piezoelectric fillers.

Efforts have been reported to address these tangled issues from filler's point of view, including (i) fabricating highly crystalline NWs as fillers (e.g., ZnO NWs [172], Li-doped ZnO NWs [173], and $BaTiO_3$ NWs [174]) due to their high crystallinity and uniform alignment in the growth direction, (ii) using organic fillers such as P(VDF-TrFE) [135] due to their better dispersion than inorganic fillers within polymer matrix, and (iii) fabricating 3D cellular-structured filler network [169]. As shown in Fig. 5(e), by fabricating PZT fillers into a ceramic foam filled with elastic PDMS, the stretchable PZT-PDMS composite possesses a continuous pathway for high-efficiency load transfer, which results in a stable and superior piezoelectric voltage of more than 60 V under a tensile strain of 15% after 5000 cycles [169]. Efforts were also reported by introducing carbon nanotubes (CNTs) as the external physical distribution disperser [175] into composites to improve filler dispersion [77,134,174]. As shown in Fig. 5(f), incorporated multiwalled carbon nanotubes (MWCNTs) into (lead magnesio niobate-lead titanate) (PMN-PT)-silicon elastomer piezoelectric composites can act as a type of physical distribution disperser [175], mechanical reinforcer, and electrical bridging agent, leading to the increased piezoelectric voltage of 4 V and current of 500 nA and meanwhile good stretchability of up to 200% as assisted by stretchable Ag nanowires-based electrodes [77]. Lastly, an optimised fabrication method such as the shear dispersion method [139,140] can mitigate the filler propagation issue, where fillers are mixed with the matrix under laminar shear force and pressure contributed by two rollers with different rotational speeds. The improved filler homogeneity allows for higher filler proportions within elastic matrix. A high filler ratio of 92 wt% has been reported in a stretchable PZT-silicone elastomer piezoelectric composite, which generated an outstanding output power density of 81.25 μW cm^{-3} under 30% strain [140].

Lastly, stretchability of piezoelectric devices can be realised by fabricating rigid piezoelectric arrays on a stretchable substrate with stretchable interconnections [170,176]. Fig. 5(g) exemplifies a PZT-based stretchable piezoelectric transducer on a PDMS substrate [170], where the stretchable serpentine structured Cu interconnections can provide the device with 25% stretchability in binary directions. On top of that, the "claw-shape" interconnections have been reported in a PZT-based piezoelectric ultrasound transducer, enabling stretchability in multiple directions, as shown in Fig. 5(h) [171].

Table 1 summarises the fabrication method, piezoelectricity, and stretchability performances of different classes of stretchable flexible piezoelectrics.

4. Self-healing

The fatigue fracture of flexible piezoelectric materials induced by cyclic mechanical loading and unloading needs to be avoided to prevent premature device failure. It is thus desirable for piezoelectric devices to be self-healing, which serves as another beneficial secondary function to boost the durability of piezoelectric energy harvesters. Current studies on self-healing piezoelectrics are still in their infancy. Self-healing property can be found in piezoelectric composites [177,178], and piezoelectric molecular crystals [179].

For piezoelectric composites, their self-healing capacity is contributed by polymer matrices, including ionomers and elastomers. Ionomers are a group of polymers with ionic functional groups attached to the polymer backbone [180]. They have been reported to be self-healing, initiated by mild thermal treatments [181]. The self-healing of

Table 1
Summary of fabrication method, piezoelectricity, and stretchability performances of stretchable flexible piezoelectrics.

Strategy	Material	Fabrication	Piezoelectricity	Stretchability	Ref
Micro-structure design	PZT on PDMS substrate	Transfer printing PZT ribbons onto prestrained PDMS substrates and releasing strain for buckled PZT	Current density of 2.5 μA mm^{-2} under periodic strain of 8%	8%	[102]
	PZT and PI layers	Transfer printing, stacking buckled PZT and PI layers	Voltage of 8.1 V with 5 PZT layers		[106]
	PVDF	Compressive buckling complex 3D microstructures	Voltage of 790 mV	~2.8%	[109]
	PVDF on PDMS substrate	Mechano-electrospinning, straight PDVF nanofibers on a prestrained PDMS substrate	Current of 1.2 nA and voltage of 40 mV with 120 PVDF fibers under 30% strain	110%	[111]
	PVDF on PET substrate	Electrohydrodynamically printing, depositing poled nanofibers onto prestrained PET substrates	Current of 4 nA and voltage of 150 mV with 50 fibres at 2.3 Hz.	100%	[112]
	PVDF on PDMS substrate with liquid metal electrode	helix electrohydrodynamic printing buckled and fractal PVDF fibres	Average maximum current of 20 nA with 120% strain	200%	[113]
	PVDF on PDMS substrate with liquid metal electrode	helix electrohydrodynamic printing self-similar PVDF nanofibers	Current of ~8 nA under 120% strain in bi-direction stretching	300%	[114]
	P(VDF-TrFE) in between of PDMS-CNT substrate and graphene	Photolithography and etching enabled micro-patterning at the interface of P(VDF-TrFE) and PDMS-CNT	Voltage up to 1.4 V under simultaneous strain and thermal gradient	30%	[115]
	P(VDF-TrFE), Ag coated nylon yarn, CNT sheets	Electro-spinning P(VDF-TrFE) nanofibres, core-shell structure with inner and outer electrodes	Voltage of 2.6 V and current of 15 nA for a single 10 mm fiber compressed laterally under 160 kPa, output density of 50 μW cm^{-3}	5%	[119]
	PVDF-TrFE nanofibers	Twisting electrospun yarns into ribbons and overtwisting into coiled structure	Voltage of 20 mV	740%	[118]
	PVDF-rGO- BT piezoelectric fibres	Melt-spinning nanofibres, twisting and coiling fibres into coiled structure	Voltage of 1.3 V and power density of 3 W kg^{-1}	100%	[117]
Morphology design	PVDF on PET substrate	Stitching PVDF straps and weaving with elastic tubes	Voltage of 51 V and power of 850 μW by stretching in lateral direction	6 mm for 9 × 9 cm^2 device	[122]
	PVDF straps	PVDF strap and fabric band twinning around elastic core forming helical structure	Voltage of 20 V at knee position	158%	[123]
	$BaTiO_3$-PVC threads	Weaving threads, Cu wires and cotton threads into fabric with interdigited electrodes	Voltage of 1.9 V and current of 24 nA at bending elbow	Arm bending	[124]
	PVDF thread	Band weaving core-shell structured PVDF thread with separated electrodes	Voltage of 3.5 V under axial strain of 0.25%, voltage of up to 8 V under wet conditions	~30%	[126]
	PVDF tattoo on Tegaderm substrate	Cut-and-paste fabrication PVDF sheets into a filamentary serpentine network	Voltage of 2.2 V with Tegaderm substrate, voltage of 2.74 V without substrate	112.9%	[9]
	PLA-SWCNT composite film	Mechanical punching process for patterning, photolithography-etching-transfer printing for device	Current of 4 nA and voltage of 210 mV under 1% strain	31%	[127]
	PVDF on Kapton substrate	Scalpel cutting for two patterns of centre cutting and edge cutting	Voltage of 299 mV at a strain level 5% for centre cutting pattern with dense spacing	30%	[131]
	PVDF film on PET substrate	Linear cutting PVDF film with FEA-guided pattern and inter-segment electrode design	Voltage of 1.63 V under 10% strain	10%	[132]
	$BaTiO_3$–P(VDF-TrFE) composite with silver electrode	Direct-write 3D printing process with designed cut shape	Voltage of 6 V under 60 N compression force and 5 Hz for T-joint-cut kirigami structure	300%	[110]
Elastic matrix	PMN-PT/CNT/PVDF	Mixing, magnetic stirring, and heating	Voltage 4 V and current 30 nA for 30 vol %PMN-PT/CNT/PVDF composite, device size 1.5 cm × 1.5 cm	6%	[134]
	$BaTiO_3$/PDMS composite with Ag NWs as electrode	Spin coating and curing	Voltage of 105 V, current density of 6.5 μA cm^{-2} and power density of 102 μW cm^{-2} for 5% filler content under 40 N periodic compression	60%	[6]
	PZT/PDMS composite	Bath sonicating and curing	d_{31} of 30 pC N^{-1} at 25% strain for 38 vol% PZT (20 μm particle size)/ PDMS (M_w = 139 kg mol^{-1})	254 ± 136% (breakage strain)	[138]
	$Pb(Mg_{1/3}Nb_{2/3})O_3$–$PbTiO_3$ microparticles, CNTs, silicone rubber matrix, and very long Ag NW electrodes	Magnetic stirring, curing, and vacuum suction method to transfer Ag NWs electrode	Voltage of 4 V and current of 500 nA under 200% stretching motion	200%	[77]
	PZT, Ag-coated glass microspheres, silicone rubber matrix.	Shear dispersion method for uniformly dispersed fillers in silicone rubber matrix	Voltage of 20 V and current of 0.55 μA with dimension of 5 cm * 4 cm under 50% strain and 0.7 Hz frequency	100%	[139]
	PZT powders in rubber matrix	Mixing technology for uniformly dispersed high-content filler	Power density of 81.25 μW cm^{-3} under 30% strain	30%	[140]
	Amino-functionalised boron nitride nanosheets/PVDF nanofibre membranes	Electrospinning and ultrasonic stirring	Voltage of 0.9 V and current of 0.85 μA for 1.5 wt% filler content	110%	[79]
	3D PZT microfoam/PDMS	PU foam template and sintering for 3D PZT microfoam, filled with PDMS	Voltage of 60 V under a tensile strain of 15% after 5000 cycles	15%	[169]

(*continued on next page*)

Table 1 (*continued*)

Strategy	Material	Fabrication	Piezoelectricity	Stretchability	Ref
Stretchable interconnection	Bulk PZT arrays with serpentine structured Cu interconnections on PI substrate	electron beam evaporation, photolithography and etching for patterning electrode, low-temperature solder paste for connection	resonant frequency of 356.6 KHz	25% in binary directions	[170]
	PZT plate with fractal serpentine Cu interconnection	Reflow soldering for bonding, low-melting point solder paste, 3D printing	Response voltage of 4256 mV with excitation voltage of 18000 mV with 5-mm transmission distance	20%	[171]

ionomers relies on the elasticity contributed by the attraction of ionic blocks, i.e., cross-linked plastics. When a fractured ionomer is heated, this elasticity can result in large-scale elongation at the fracture region to heal/close the crack, realising the self-healing function [180]. As the matrix of piezoelectric composites, ionomers are also flexible, mechanically robust, and possess good adhesion to ceramic piezoelectric fillers. James et al. [177] incorporated PZT powders into a Zn ionomer and reported excellent fatigue resistance at strain levels of 4%. For high strains of 6% and 8%, the loss of piezoelectric charge coefficient d_{33} due to fracture occurrence can be partially recovered under a thermal treatment at 70 °C for 40 min (roughly 92% and 73% at 6% and 8% strains, respectively).

Elastomers are another type of self-healing matrices of piezoelectric composites. Compared with the above ionomers, elastomers may self-heal without external stimulus at room temperature. The self-healing property of various elastomers stems from different mechanisms depending on their chemical structures and polymerisation processes. Yang et al. [178] reported a self-healing PDMS-4,4′-methylene bis phenyl urea $(MPU)_x$-isofordone biuret $(IU)_{1-x}$ supramolecular elastomer as the matrix of piezoelectric PZT particles. Its self-healing property stems from a dynamic hydrogen bond network composed of alternating strong and weak hydrogen bonds, as shown in Fig. 6(a). The strong hydrogen bonding from MPU can provide a highly tensile property to improve the elasticity of the elastomer, while the weak hydrogen bonding from IU contributes to the self-healing of fractures at room temperature. By repeatably cutting the device, an almost full recovery of the device output was observed. At 70 wt% PZT content, the output voltage and current of the device reached peak values of 3.2 V and 56.1 nA, respectively [178].

Methyl thioglycolate–modified styrene–butadiene–styrene (MGSBS) is another type of self-healing elastomer [182]. Unlike the above hydrogen bonding mechanism, its self-healing behaviour originates from the δ+ protons adjacent to the ester of methyl thioglycolate that electrostatically interact with the δ-aromatic centre of styrene, as shown in Fig. 6(b). MGSBS can withstand the damage of 18 mm cut line and be self-healed after 24 h. By integrating a piezoelectric macrofiber composite with MGSBS, a leaf-shape self-sensing piezoelectric actuator was fabricated with a high bandwidth up to 10 kHz, which is promising to be applied to novel soft robotics.

Self-healing property can also be realised by reducing the crystallinity of elastomers, and a self-healing lactate-based piezoelectric elastomer (LBPE) has been reported using this strategy [183]. As shown by the chemical structure of the elastomer in Fig. 6(c), the reduced crystallinity is attributed to butanediol (BDO) and sebacate (SA) as flexible

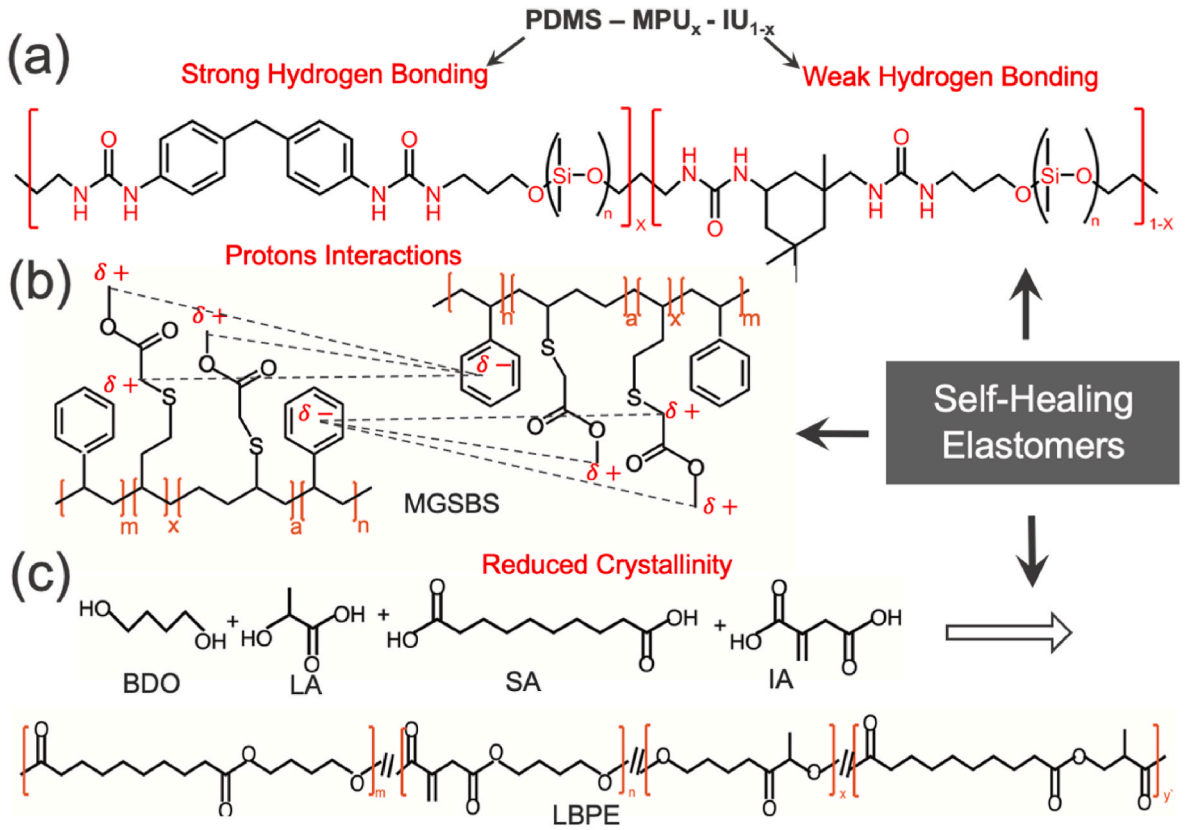

Fig. 6. The mechanisms of self-healing elastomers for piezoelectric composites. Self-healing (a) polydimethylsiloxane (PDMS)-4,4′-methylene bis phenyl urea $(MPU)_x$-isofordone biuret $(IU)_{1-x}$ due to dynamic hydrogen bond network [178], (b) methyl thioglycolate–modified styrene–butadiene–styrene (MGSBS) due to proton interactions [182], and (c) lactate-based piezoelectric elastomer (LBPE) due to reduced crystallinity [183].

chains and itaconate (IA) as a cross-linking agent. The reduced crystallinity enables larger lattice distortions and asymmetries and therefore reduced elastic modulus to withstand external forces. Meanwhile, its low glass transition temperature and long linear molecular nature enable self-healing capability from irregular scratches.

The above self-healing capacities are enabled by soft and amorphous polymers as matrices. Lately, self-healing behaviour was also observed in crystals. Bhunia et al. reported a self-healing piezoelectric bipyrazole organic single crystal [179], whose crystal structure is shown in Fig. 7. A 3D hydrogen-bonded network can be found between water and bipyrazole molecules, as well as the N–H···N interactions within the packing of bipyrazole molecules. This hydrogen-bonded network contains dispersive interactions, leading to highly elastic deformations at fractures. Meanwhile, breaking the polar molecular arrays generates opposite electrical charges on the fracture surfaces due to the formation of molecular dipoles, which act as a natural restoring force at the fracture area to drive the self-healing process. Although the flexibility of elastic molecular single crystals is inferior to other polymer-based self-healing piezoelectric composites, their high crystallinity is promising to generate high piezoelectric outputs. Moreover, their superior atomic-level self-healing may be favourable for flexible electronics with micro-components based on accurately oriented and highly crystalline piezoelectric materials.

5. Hybrid energy harvesting

It is vital to ensure the continuous and stable energy generation of flexible piezoelectric devices under complex working environments, especially given conditions with inadequate mechanical energy supply. The solution may be obtained by considering the compensation effect of other types of energy harvesting to generate power collectively and possibly synergistically with piezoelectric systems. By integrating other energy harvesters into flexible piezoelectric devices, various energy sources can compensate each other to contribute to a continuous and stable energy output whenever at least one of them is available, as schematically shown in Fig. 8(a). In fact, apart from piezoelectric-responsive mechanical energy, other types of energy sources such as friction-related mechanical energy, thermal energy, and solar energy can also be harvested respectively by triboelectrics [184,185], thermoelectrics [186–188] or pyroelectrics [189,190], and photovoltaics [191–193], to generate electrical power. This section focuses on the fundamental mechanisms and structures to synergistically integrate flexible piezoelectric generators with other energy harvesting systems to develop the secondary function of hybrid energy harvesting.

5.1. Comprehensive mechanical energy harvesting

Mechanical energy is abundant in our daily life, and the energy induced by pressing, bending, stretching, and twisting can be harvested by piezoelectric materials. In addition, other types of mechanical energy induced by rubbing different materials in contact can also be harvested by triboelectricity. Compared with piezoelectric materials, triboelectric materials do not have to be dielectric and have a much wider range of material choices, more diverse working modes (e.g., contact-separation mode, sliding mode, single-electrode mode, and freestanding mode) [194], and higher energy generation efficiencies under low-frequency motions [185]. By inducing synergistic integration, the hybrid generator can produce outputs beyond the linear summation of the outputs of the individual triboelectric and piezoelectric mechanisms [195], thereby realising a comprehensive mechanical energy harvester for continuous energy generation.

The mechanism of the triboelectric effect lies in the coupling effects of contact-electrification and electrostatic induction, by which certain materials will be charged by contact-electrification charges after contacting a different material, and then being separated [196]. The charges on the contact-separation surface tend to subsequently induce an equal number of opposite charges on the surface away from the contact-separation surface by electrostatic induction. In this way, if the

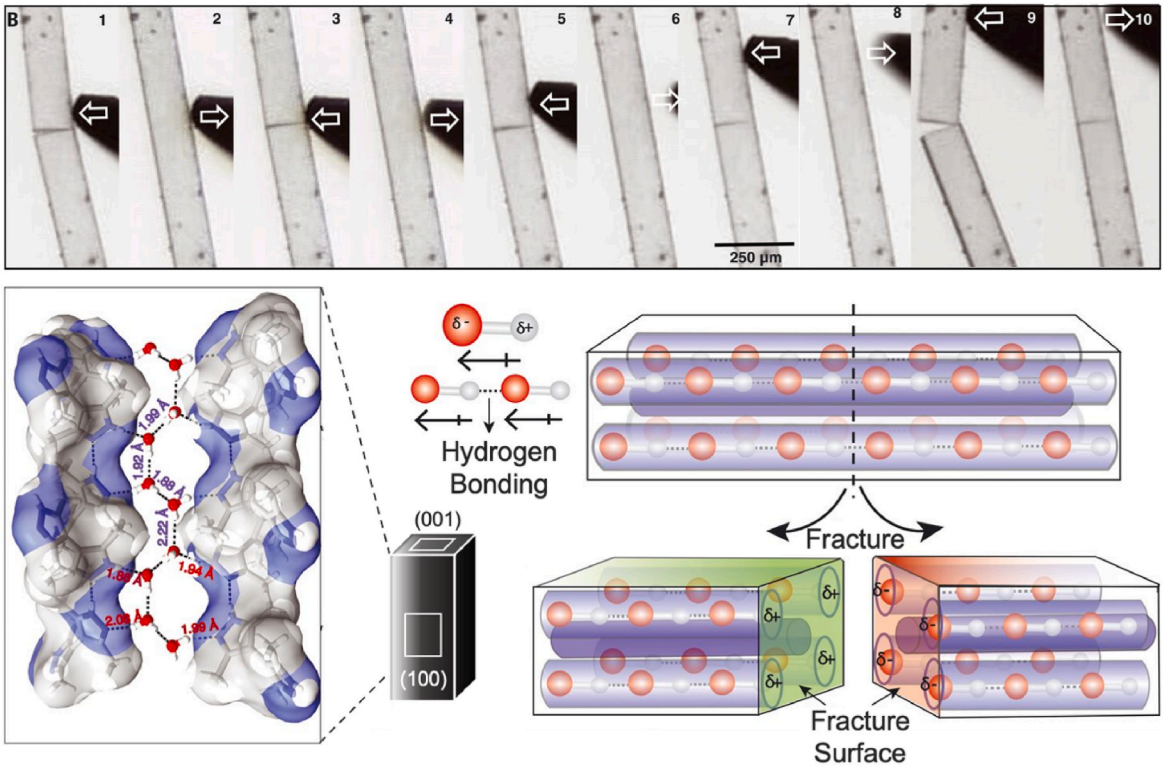

Fig. 7. Self-healing piezoelectric crystals. Piezoelectric bipyrazole organic crystals with an electrostatically driven self-healing capacity [179]. Reproduced with permission [179]. Copyright 2021, American Association for the Advancement of Science.

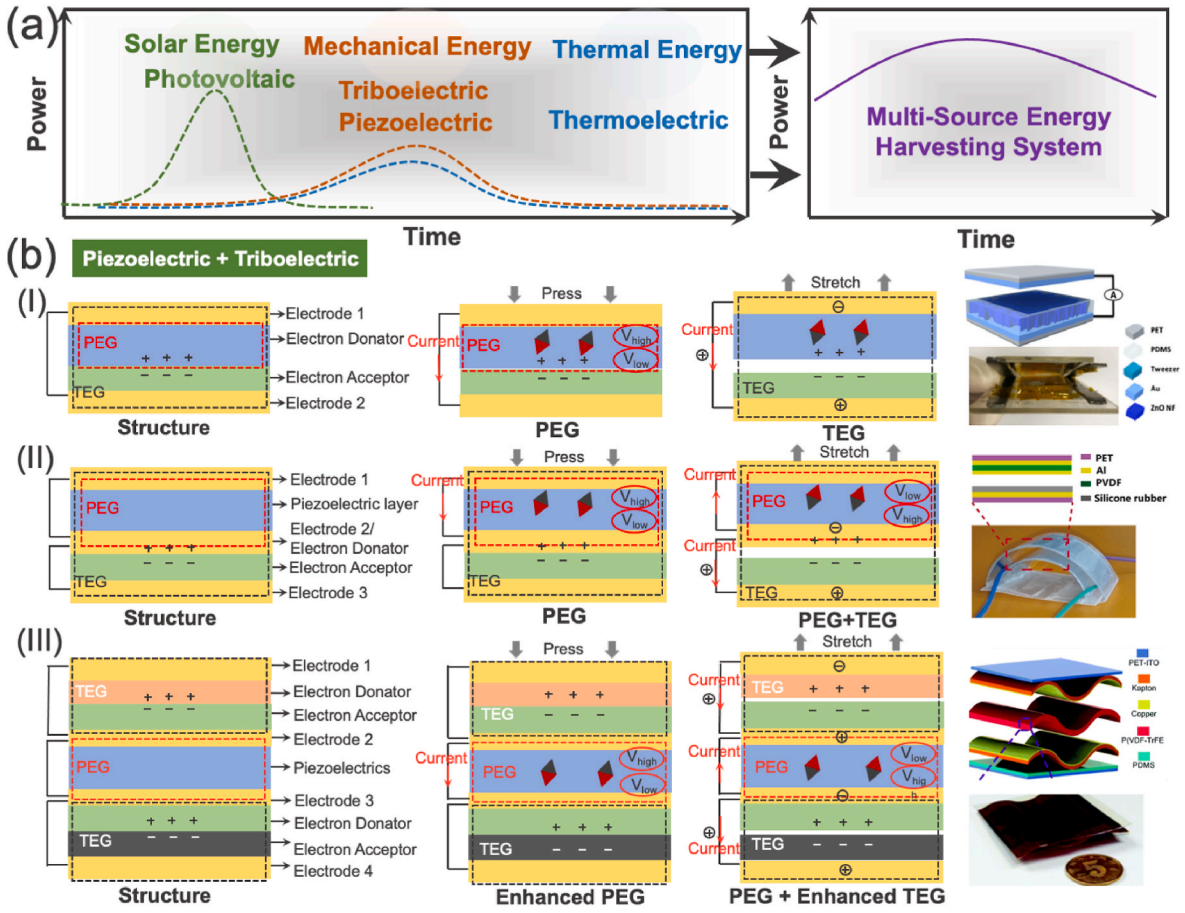

Fig. 8. Mechanisms and structures to integrate flexible piezoelectric and triboelectric energy generators. (a) The schematic of continuous energy harvesting by piezoelectrics and triboelectrics (mechanical energy), thermoelectrics and pyroelectrics (thermal energy), and photovoltaics (solar energy). (b) Three typical mechanisms and structures to synergistically integrate flexible piezoelectric and triboelectric generators. The example of Structure (I) is reproduced with permission [199]. Copyright 2018, American Chemical Society. The example of Structure (II) is reproduced with permission [202]. Copyright 2017, Elsevier. The example of Structure (III) is reproduced with permission [203]. Copyright 2017, Royal Society of Chemistry.

electrostatically induced surfaces of the two materials are connected, triboelectric currents will be driven to flow externally. The triboelectric potential and current can be derived by the following two equations:

$$V_T = -\frac{\rho_T d}{\varepsilon_0} \quad \text{(Eq. 5.1)}$$

$$I_T = C_T\frac{\partial V_T}{\partial t} + V_T\frac{\partial C_T}{\partial t} \quad \text{(Eq. 5.2)}$$

where V_T and I_T are triboelectric voltage and current, respectively, ρ_T is the triboelectric charge density, ε_0 is the vacuum permittivity, and d is the distance between two triboelectric materials.

The outputs of piezoelectricity and triboelectricity are related, i.e., piezoelectric voltage and triboelectric charges, respectively. Their integration can be simply realised by replacing the triboelectric layer of a triboelectric energy generator (TEG) with a piezoelectric material, or a tribo-piezoelectric composite (piezoelectric fillers within a triboelectric matrix) [197]. The typical structure of tribo-piezoelectric hybrid energy generators can be understood as the structure (I) of Fig. 8(b), where electron donator and accepter depict the positively and negatively charged materials of TEG after a contact-separation motion, respectively. When the hybrid device is pressed, the piezoelectric energy generator (PEG) will be firstly triggered, generating a piezoelectric voltage and thus a piezoelectric current flowing from electrode 1 to 2. Meanwhile, the contact-electrification charges appear at the contact interface of TEG. Afterwards, the separation of TEG contact surfaces induced by stretching or rubbing leads to electrostatically induced charges on the surfaces of electrodes 1 and 2. By externally connecting the two electrodes, a triboelectric current can flow from electrode 1 to 2. As a result, by cyclically pressing and stretching the hybrid device, the PEG and the TEG can work collectively to harvest comprehensive mechanical energy. Chowdhury et al. [197] utilised this structure to fabricate a Li-doped ZnO-PDMS-based flexible piezoelectric-triboelectric hybrid energy generator, and realised a continuous electricity generation of 60.0 V potential (compared with 10.1 V from sole Li-doped ZnO-PDMS-based PEG [198]) and 75 μA current without electrical poling. Similarly, He et al. [199] fabricated a ZnO-PDMS-based piezoelectric-triboelectric hybrid energy generator with Structure (I), but the piezoelectric ZnO layer is encapsulated with Au to realise pronounced triboelectrification of Au–PDMS contact, as shown on the right of Structure (I). The hybrid generator can produce a peak output voltage of ~470 V and a current density of ~60 μA cm^{-2}, lighting up 180 commercial light-emitting diodes through periodic hand compression. In contrast, the output voltage and current density of sole Zn-PDMS-based PEG is only 130V and 37 μA cm^{-2} under the same testing condition (i.e., 7 N periodic compression under a frequency of 10 Hz).

It can be noted that stretching processes in structure (I) only output triboelectric currents, while the as-induced piezoelectric voltage is wasted due to the absence of an electrode in PEG. The structure (II) shown in Fig. 8(b) can harvest both triboelectric and piezoelectric currents during stretching processes by adding one electrode (electrode 2 in yellow colour) in between that of the electron donator and the electron

acceptor of the above-described structure (I). In this way, PEG and TEG are connected in parallel. When the hybrid device is pressed, piezoelectric current can still be generated as discussed above, flowing from electrode 1 to 2. But when the device is stretched, electrode 2 can both act as an electron donator in TEG leading to a triboelectric current flowing from electrode 2 to 3, and also as an electrode of PEG to output a piezoelectric current from electrode 2 to 1, resulting in an increased overall power output. Jung et al. [200] applied Structure (II) to fabricate a PVDF (piezoelectric)-PTFE (triboelectric) hybrid energy which can light 600 LED bulbs with 0.2 N pressing force. The high output can be attributed to the designed arc-shaped PEG in this hybrid system to induce higher levels of strain and drive PEG to contract. Under the same testing condition and device size (7×3 cm^2), great enhancements of output voltage and current density were observed from the hybrid device (370 V and 12 μA cm^{-2}) than sole PEG (80 V and 7.62 μA cm^{-2}). Wang et al. [201] tried to optimised the hybrid system from TEG point of view, by which they introduced pillar micro-patterns onto the surface of triboelectric MWCNT- PDMS membrane in order to increase the surface roughness to improve the triboelectric output. The TEG output was reported to be improved from 20.08 V to 30.06 V after patterns introduction. Zhu et al. [202] combined the above two strategies and further optimised the arc structure to a double-arched structure, where both PEG and TEG were designed to be arc-shaped, to develop a piezo-tribo hybrid sensor, as shown on the right of Structure (II). The d-arched sensor with middle shared electrode (the electrode 2 in Structure (II) schematic) can increase sensitivity and deformation range, while micro-patterns on the surface of silicon rubber can benefit TEG with improved output. Consequently, the d-arched hybrid sensor was able to present output voltage of 34.6 V and current of 6.6 μA under the vibration amplitude of 6 mm. Correspondingly, the output of sole PEG was observed to be 24.2 V and 5.3 μA.

The above two structures both require the incorporation of one dielectric piezoelectric material into TEG. Structure (III) in Fig. 8(b) can overcome this restriction by alternatingly connecting PEGs and TEGs, where the top and bottom TEGs are connected with one PEG in the middle. Different with the independent working mechanisms of PEG and TEG in the above two structures, this structure allows a mutual output reinforcement. Specifically, when the hybrid is pressed, the materials adjacent to PEG (highlighted as green) are designed to be an electron acceptor and an electron donator of the top and bottom TEGs, respectively, to possess opposite contact-electrification charges. This, in turn, poses an electrical field to the middle PEG. If the direction of piezoelectric voltage upon pressing is the same as this electrical field, a TEG-reinforced piezoelectric output can be achieved for the PEG. On the other hand, when the hybrid is stretched, the piezoelectric voltage of PEG can impose a high/low electric potential to the adjacent triboelectric layers (highlighted as green), which can strengthen the electrostatic induction of TEG and leading to PEG-enhanced triboelectric currents. Chen et al. [203] employed Structure (III) and adopted a wave-shaped structure to fabricate a piezo-triboelectric hybrid generator based on P(VDF-TrFE) nanofibers, as shown on the right of Structure (III). Such a wavy structure has the advantages of built-in space and self-recovery characteristics. The peak hyrid output and current were observed to be 96 V and 3.8 μA respectively, showing around two times improvement than its initial piezoelectric output. Meanwhile, due to the reinforcement effect of piezoelectric potential towards TEG, as described above, the output of TEG was observed to increase by 16 V.

5.2. Mechanical and thermal energy harvesting

The human body can provide continuous and stable thermal energy to be harvested for power generation. So far, pyroelectrics and thermoelectrics have been reported as two types of thermal energy harvesters. Pyroelectric materials are a group of piezoelectric materials (dielectrics) that can generate a voltage across the material in the presence of a thermal fluctuation. The mechanism of pyroelectricity is similar to piezoelectricity. However, rather than mechanically induced, dipole moments and polarisation are thermally induced, causing atoms to oscillate beyond their neutral positions under a temperature fluctuation [204]. Since all pyroelectric materials are also piezoelectric, their integration can be essentially understood as fabricating "piezoelectric" generators using pyroelectric materials [87,115,205–207]. For example, Lee et al. [115] fabricated a pyro-piezoelectric hybrid generator with a typical sandwich structure, i.e., piezoelectric and pyroelectric P (VDF-TrFE) film in the middle of two stretchable electrodes. By simultaneously applying stretching and heating, increased output of 1.1 V was observed, in contrast to that of 0.7 V and 0.4 V under only stretching and heating conditions, respectively.

Thermoelectric materials can realise the reliable and direct conversion between heat and electricity through the Seebeck effect (power generation) and the Peltier effect (refrigeration) [208]. The mechanism of thermoelectric materials can be understood by the diffusion of charge carriers from the hot end to the cold end in the presence of a temperature difference, which forms an electric voltage between two ends of the thermoelectric material, and vice versa [186,208–210]. The performance of a given thermoelectric material is governed by the dimensionless figure of merit (zT), which is expressed as:

$$zT = \frac{S^2 \sigma T}{\kappa} \quad \text{(Eq. 5.3)}$$

where S, σ, κ, and T are the Seebeck coefficient, electrical conductivity ($\sigma = n\mu e$, where n, μ, and e are the carrier concentration, carrier mobility, and electron charge, respectively), total thermal conductivity, and absolute temperature, respectively.

The efficiency of a given thermoelectric energy generator, on the other hand, can be evaluated by:

$$\eta_p = \frac{T_h - T_c}{T_h}\left[\frac{\sqrt{1+zT_{ave}}-1}{\sqrt{1+zT_{ave}}+T_c/T_h}\right] \quad \text{(Eq. 5.4)}$$

where η_p, T_h, and $T_c$are the power-generation efficiency, and the temperatures at the hot and cold ends, respectively; and $zT_{ave}$is the average dimensionless figure of merit (zT) which is calculated by:

$$zT_{ave} = \frac{1}{T_h - T_c}\int_{T_c}^{T_h} zT\mathrm{d}T \quad \text{(Eq. 5.5)}$$

The uncoupled working mechanisms of thermoelectric and piezoelectric materials favour their facile integration for continuous energy generation. Additionally, thermoelectric materials enable precious temperature control, including cooling effect below ambient temperature by controlling external voltage input, which is promising for a medical cooling blanket and may benefit biomedical technologies such as polymerase chain reaction (PCR) [211]. Therefore, integrating thermoelectric energy harvesters with flexible PEGs holds promises to not only realise continuous energy outputs by simultaneously harvesting the thermal and mechanical energy of the human body, but also enable novel applications of PEGs in biomedical settings.

Current high-performance inorganic thermoelectric materials for room-temperature energy harvesting, e.g., Bi_2Te_3-based thermoelectric materials [212,213], are toxic and too rigid to be integrated with flexible PEGs. To overcome the above issues, a biocompatible encapsulation layer is required, and miniatured thermoelectric blocks are preferred to alleviate their geometrical incompatibility with flexible PEGs. Kumar et al. [214] integrated thermoelectric and piezoelectric generators by embedding miniatured Bi_2Te_3 and Sb_2Te_3-based thermoelectric blocks into a piezoelectric PVDF-ZnO encapsulation, as shown in structure (I) in Fig. 9(a). By hand tapping the hybrid generator under a temperature difference of 4 K, the thermoelectric and piezoelectric generators can output power of ~1.8 nW and ~1.2 μW, respectively. The low thermoelectric output may be associated with the PVDF-ZnO encapsulation, due to its adverse effect on heat transfer that prevents the maintenance

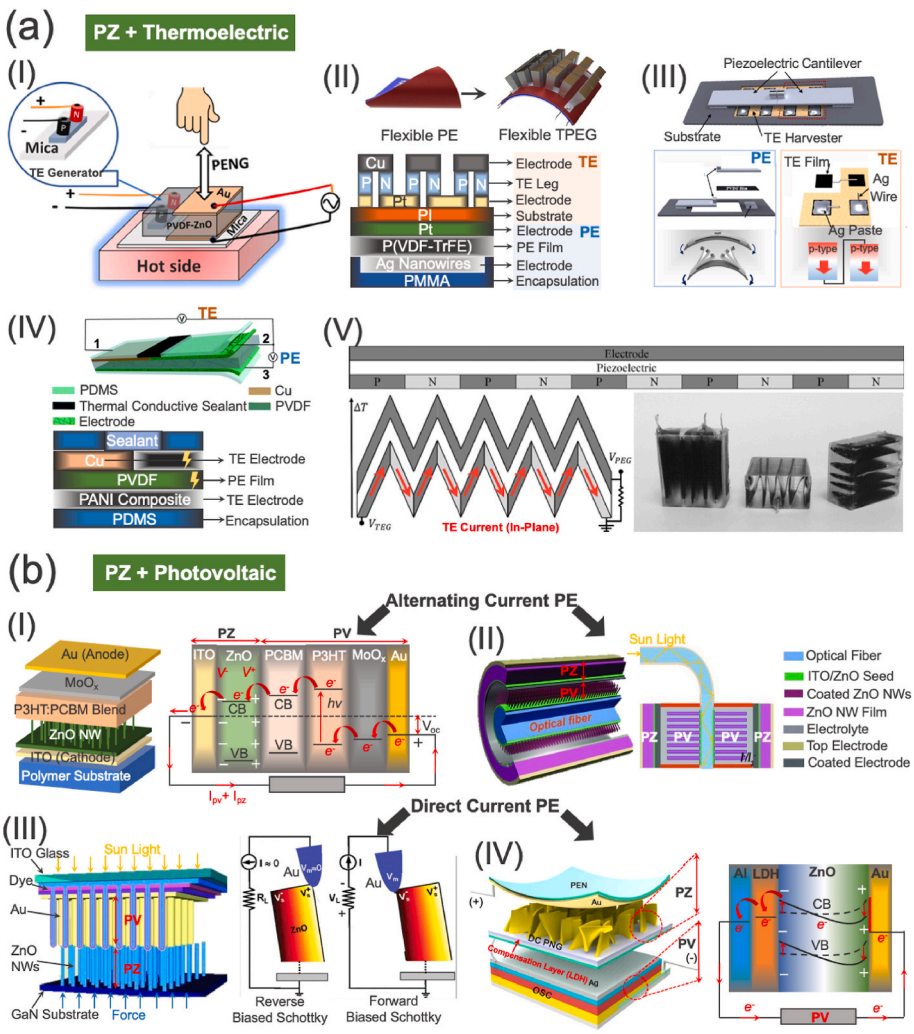

Fig. 9. Mechanisms and structures to integrate flexible piezoelectric generators with thermoelectric or photovoltaic generators. (a) Integrating piezoelectric and thermoelectric generators with structures (I) [214], (II) [216], (III) [220], (IV) [223], and (V) [222]. (I) Reproduced with permission [214]. Copyright 2019, Elsevier. (II) Reproduced with permission [216]. Copyright 2021, Elsevier. (III) Reproduced with permission [220]. Copyright 2019, Springer Nature. (IV) Reproduced with permission [223]. Copyright 2019, Royal Society of Chemistry. (V) Reproduced with permission [222]. Copyright 2016, American Institute of Physics. (b) Integrating photovoltaic cells with alternating current (AC)-type piezoelectric generators with structures (I) [224] and (II) [225], and with direct current (DC)-type piezoelectric generators with structures (III) [226] and (IV) [227]. (I) Reproduced with permission [224]. Copyright 2011, Royal Society of Chemistry. (II) Reproduced with permission [225]. Copyright 2012, Wiley-VCH. (III) Reproduced with permission [226]. Copyright 2011, Wiley-VCH. (IV) Reproduced with permission [227]. Copyright 2015, Elsevier.

of the necessary temperature difference for thermoelectric power generation.

Optimised structures were reported by Lee et al. [215] and Kim et al. [216] by stacking flexible inorganic thermoelectric generators with PEGs. Their structures can be understood by structure (II) in Fig. 9(a), where miniatured Bi_2Te_3-based thermoelectric blocks were fabricated on a flexible polyimide (PI) substrate and integrated with a P(VDF-TrFE) film-based PEG underneath [216]. By optimising the surficial properties of thermoelectric and piezoelectric components, a hybrid current of 3.8 μA was generated under a temperature difference of 3 K and periodic bending, compared with that of 1.5 μA contributed by only PEG. However, the flexibility of this structure is still restricted by the rigid thermoelectric generator and the contact between the thermoelectric blocks and flexible substrate.

More flexible thermo-piezoelectric hybrid generators can be achieved by utilising thermoelectric thin films [217–219]. Structure (III) in Fig. 9(a) depicts a novel structure to realise this goal [220]. Basically, two PVDF-based piezoelectric cantilevers are combined with flexible Sb_2Te_3-PEDOT:PSS thermoelectric paste on a flexible substrate. Without mechanical loadings, the two cantilevers are magnetically attracted by permanent magnets. When a mechanical bending is applied and its force is larger than the magnetic force, the two cantilevers can be separated and rapidly vibrate at their natural frequencies. Meanwhile, the underlying thermoelectric generator can harvest thermal energy without being interfered. The average power densities of piezoelectric and thermoelectric generators were 28.57 and 0.64 μW cm^{-2} (given a 9.2 K temperature difference), respectively. Although the thermoelectric output is much lower than that of the piezoelectric generator, the thermoelectric energy output was continuous, contributing to an uninterrupted total energy output [220]. The drawback of this structure, however, can be traced in its cantilever design that limits the mechanical energy harvesting of low-frequency motions.

The utilisation of thermoelectric thin films suffers from concerns of poor thermoelectric performances [221] and inferior temperature differences maintained in the out-of-plane direction, which restrict their energy harvesting. To address the above concerns, novel structures were proposed by Montgomery et al. [222] and Zhu et al. [223] to take advantage of the superior in-plane thermoelectric properties of thin films to fabricate thermo-piezoelectric hybrid energy generators. These structures, as shown in structures (IV) and (V) in Fig. 9(a), use thermoelectric materials as the electrodes of PEG. For structure (IV), a three-phase Te-MWCNT/polyaniline (PANI) thermoelectric composite with a relatively good electrical conductivity of 196 S cm^{-1} and a thermopower of 66.4 mV K^{-1} was applied as the electrode of PVDF-based PEG [223]. As shown, when the heat was transferred to the top thermoelectric electrode through the black thermal conductive sealant, it flows in a horizontal/in-plane rather than an out-of-plane manner in the material. A temperature difference will thus exist at the two ends of the electrode, generating electricity conducted by copper wires 1 and 2 attached by silver paste. If vertical mechanical stress is further applied to the device, PVDF film can output piezoelectric power through copper wires 2 and 3, realising the hybrid energy harvesting of

thermal and mechanical energy. By approaching a warm heat block of 37.8 °C to the hybrid device, a thermoelectric voltage of 0.45 mV was generated to compensate the piezoelectric voltage of 1.35 V under a periodic compression force of 5 N [223].

The scale of thermoelectric thin films in Structure (IV) is constrained as an electrode, which directly causes its low output. Structure (V) is suitable for applications requiring a larger usage of thermoelectric thin films, where zigzag structured thermoelectric electrode has been designed [222]. One end of the thermoelectric thin film (CNT-PVDF) is connected in series to the piezoelectric film (PVDF) as the bottom electrode of the top PEG, while the other end is connected to the bottom of the hybrid device, forming the zigzag design. The temperature difference is forced along the in-plane direction to achieve a larger thermoelectric output. The device was observed to generate additional ~3 mV thermoelectric voltage under a 10 K temperature difference on top of piezoelectric voltage. The hybrid system can generate 5.3 times higher voltage (28 μV Pa^{-1}) than a conventional flat structure under an out-of-plane pressing condition and a 10 °C temperature difference [222].

5.3. Mechanical and solar energy harvesting

The sun is the most abundant renewable energy in the world; the solar energy which the earth receives in an hour is more than the energy consumed in a year [228]. Photovoltaic cells have long found success in harvesting abundant solar energy with relatively higher energy efficiency than other energy harvesting systems [229–232], and their applications in biomedical settings have been reported to produce substantial energy to power most wearable biomedical devices [233]. In terms of biomedical implants, biocompatible and even bioresorbable photovoltaic cells [234] can serve as implantable subdermal energy generators producing higher output than PEG (100–200 μW mm^{-2} than PEG's 0.4–30 μW mm^{-2} [235]). Therefore, integrating photovoltaic materials with PEG is promising to compensate for the low and unstable power output from solely PEG, while PEG can compensate for solar cell's energy shortage under poorly light-accessible conditions (e.g., rainy days or dark environments) by harvesting mechanical energy, which collectively contribute to the continuous energy output of hybrid energy harvester.

The working mechanism of a photovoltaic cell is the photovoltaic effect, which converts solar energy into electricity [236]. A photovoltaic cell contains a p-n junction created by two contacted n- and p-type semiconductors. Electrons and holes tend to diffuse in the p-n junction, forming a potential barrier, i.e., the depletion zone, near the interface, pointing from n-type material to p-type material. When sunlight strikes a photovoltaic cell, charge carriers are activated by photon energy. The free electrons are then directed by the potential barrier to flow into the n-type region, while free holes are directed into the p-type region. The separation of charge carriers creates a potential difference across the p-n junction to generate direct current (DC) through an external circuit.

The power conversion efficiency (PCE) of photovoltaic cells can be calculated by the following equation:

$$\eta_{solar}(\%) = \frac{P_{max}}{P_{in}} = \frac{V_{oc} \times J_{sc} \times FF}{P_m} \times 100 \quad \text{(Eq. 5.6)}$$

where $P_{max}$is the maximum output performance, $P_{in}$is input solar energy, V_{oc} is the open-circuit voltage, J_{sc} is the short-circuit current, and FF is the fill factor which represents the maximum power from the solar cell, obtained from the *I–V* curve.

Since the energy harvesting of photovoltaic and piezoelectric generators are independent, they can be integrated by facilely assembled. For example, a hybrid generator fabricated by depositing a ZnO-based quantum dots photovoltaic cell onto a PVDF-based PEG and has been reported to simultaneously harvest ultraviolet light and mechanical energy, and exhibit a maximum power density of 0.97 mW cm^{-3} [237]. The integration of solar cell greatly enhanced the output voltage and current of PEG from 0.23 V to 0.36 V and 3.4 μA to 9.29 μA, respectively. Similarly, a hybrid generator with a P3HT-based photovoltaic cell deposited on a PVDF piezoelectric film was reported to have a peak power of 85 μW under a solar simulator and a wind speed of 10 m s^{-1} [238]. Another integration method has been reported to assemble leaf-shaped photovoltaic and piezoelectric components into a tree-shaped hybrid system [239]. Such a structure does not require deposition techniques to be fabricated and can output a maximum power output of 3.42 mW (1.29 mW from 110 mm × 50 mm solar cell film under 2 kΩ loading resistance). However, the random movements of piezoelectric components require additional rectifiers, i.e., a full wave bridge rectifying system, to rectify and integrate the harvested energy from each piezoelectric component, which might electrically complicate the hybrid system.

The above structures are based on separated photovoltaic cells and PNGs. Nevertheless, because photovoltaic cells are composed of semiconductor materials, the integration can also be realised by fabricating photovoltaic cells directly using piezoelectric semiconductors. Non-toxic ZnO are n-type semiconductors with piezoelectric properties [240]. Therefore, piezoelectric ZnO can be a natural candidate to be integrated with photovoltaic cells, utilising its coupled piezoelectric and photovoltaic properties. The Structure (I) in Fig. 9(b) shows a naturally integrated photovoltaic-piezoelectric hybrid generator using n-type ZnO NWs and p-type P3HT-based blend [224]. When enough photon energy (*hv*) is imparted to the photovoltaic cell, electrons in the valence band are activated into the conduction band and subsequently flow from high to low work functions within the cell. Meanwhile, if mechanical stress is applied to induce a piezoelectric voltage in ZnO NWs pointing from the p-n junction (V^+) to the cathodic ITO (V^-) (leading to positive piezoelectric pulses), the total output is reinforced. However, negative piezoelectric pulses may offset the photovoltaic current. Therefore, the mechanical straining of piezoelectric ZnO in this structure needs to be programmed to prevent full strain recovery after bending, leading to outperformed positive pulses than the negative pulses.

The photovoltaic cells in the above structures require the exposure of adequate ambient lighting to function properly, but this might be a challenge under certain circumstances, such as rainy days or dark environments. The Structure (II) in Fig. 9(b) mitigates this challenge by using a novel core-shell optical fibre structure that allows the remote transmission of light even in concealed or light-deprived conditions [225]. Such a core tunnel structure enables the reinforcement of sunlight transmission to impart sufficient photon energy to the inner dye-sensitized solar cell. By applying a cyclic pressure on the outer ZnO PEG, a piezoelectric alternating current (AC) can be generated, producing output of 7.65 μA (piezoelectric current of 0.13 μA) and 3.3 V (piezoelectric voltage of 2.9V) with a diameter of 500 μm and a length of 2 cm fibre.

Without external rectifiers, it should be noted that the total output is only enlarged when the polarity of piezoelectric voltage is the same as the photovoltaic voltage. The incompatibility between piezoelectric AC and photovoltaic DC needs to be overcome to develop a high-performance hybrid system.

The challenge of AC-DC incompatibility may be solved by the Schottky barrier [241], where the piezoelectric output can be transformed from AC to DC by rectifying metal-semiconductor interfacial current transports. The formation of a Schottky barrier occurs when a metal is put in direct contact with a semiconductor and the difference between the metal's work function and the semiconductor's electron affinity is sufficiently large. The Schottky barrier can act as a "gate" to allow electron flow from high to low energy states (forward bias) while blocking the opposite or backflow of electrons (reverse bias), as shown in the schematic of Structure (III) in Fig. 9(b). By forming a Schottky barrier between a piezoelectric semiconductor and a metal electrode, the AC-type piezoelectric current can be rectified without requiring external rectifying components.

The application of Schottky barrier in piezoelectric-photovoltaic hybrid can be found in Structure (III) in Fig. 9(b), where a "teeth-to-teeth" structure presents between a ZnO NWs-based solar cell (top) and a ZnO NWs-based PEG (bottom) [226]. When mechanical vibrations are imposed, mechanical contact between the top Au-coated ZnO NWs and the bottom piezoelectric ZnO NWs can generate AC-type piezoelectric currents. Due to the different work functions of Au and ZnO, a Schottky barrier can be formed between Au and ZnO to rectify piezoelectric output from AC to DC, which can subsequently merge with photovoltaic currents to enhance the hybrid output. Under full sunlight illumination, this hybrid generator's output power density was 34.5 μW cm^{-2}, among which an increment of 32.5 μW cm^{-2} was contributed by solar cell.

Another strategy to realise DC-type piezoelectric output involves introducing a compensation layer at the interface of piezoelectric layer and electrode [242]. Structure (IV) in Fig. 9(b) depicts a Zn–Al double hydroxide (LDH) compensation layer between piezoelectric ZnO nanosheets and underlying Al electrode [227]. When the ZnO nanosheets are mechanically pressed, the positive charges in the LDH layer can compensate for the interfacial electrons of ZnO. Huge negative charges can thus accumulate at the ZnO-LDH interface, creating a high DC-type potential difference to rectify piezoelectric currents. The device can continuously output a hybrid voltage of 0.71 V with DC-type pulses under light illumination and periodical mechanical pressures, from which 0.56 V was contributed by the solar cell.

Hybrid energy generators with more than two energy harvesting techniques have also been proposed to simultaneously harvest multiple energy sources [243,244]. An impressive tribo-pyro-photo-piezoelectric hybrid generator has been reported to realise a continuous energy supply using mechanical, thermal, or solar energy sources, with peak voltage and current output of 80 V and 5 μA, respectively [244]. Indeed, integrating other energy harvesters into PEG is a promising strategy to scavenge multiple energy sources and contribute to continuous and reliable power supply under various circumstances.

6. Conclusion, challenge, and outlook

Flexible piezoelectrics can sustainably harvest mechanical energy from the human body by conformally attaching onto curvilinear human body. To boost their biomedical energy harvesting, some secondary functions are desired to address or mitigate issues that merely improved piezoelectric efficiencies cannot answer. This review systematically summarised secondary functions of stretchability, hybrid energy harvesting, and self-healing for flexible piezoelectrics by providing insights into mechanisms and strategies for function development and unravelling the link between structural characteristics and properties. Our work aims to emphasise the significance of these secondary functions in the practical applications of flexible piezoelectrics, and hopefully inspire more future work on this aspect.

Despite fruitful progresses, challenges remain to develop secondary functions, and they are desired to be solved or ascertained. Solutions might arise from the cross-field collaborations between piezoelectricity and other fields, including state-of-the-art manufacturing technologies, computational simulations, and advanced microscopies. Herein, the challenges and the corresponding outlooks to develop secondary functions of flexible piezoelectrics are proposed, which may serve as a reference for future work.

(1) **Stretchability.** To advance the commercialisation of stretchable piezoelectrics, wireless communication is highly desired, which can be realised by radio frequency (RF) system-based stretchable sensing platform [245] and standalone stretchable device with 3D stretchable microstrip antennas [246,247]. Future endeavours need to consider improving the durability and reliability of not only stretchable piezoelectric material but also the stretchable electrode/interconnection, circuit, and substrate/encapsulation as a whole. In addition, the wearability of stretchable piezoelectrics can be user-specific as the Young's modulus of human skin tend to increase with age. It has been reported that stretchability with an elastic modulus close to the elastic modulus of human skin would lead to more comfortable wearing experience, while with lower Young's modulus than that of human skin may lead to better skin feeling in touch [248]. A standardised evaluation criterion is expected to be devised to guide the design of wearability for customer-oriented product development. Lastly, since piezoelectric responses are closely related to load transfer and distribution, advanced mechanics models are required to design stretchable piezoelectrics with complex 3D stretchable structures.

(2) **Hybrid energy harvesting.** Unexpected function interference between different energy systems needs to be considered or avoided for integrated hybrid energy harvester. For example, (i) the cyclic strains required by PEGs may be adverse to the temperature maintenance of thermoelectric generators due to the self-heating effect of stacked piezoelectric layers [249], (ii) the strain may also induce the strain effect [250] in thermoelectric materials to affect local heat flux distribution, which in turn affect thermoelectric and photovoltaic energy harvesting, (iii) the interface between different energy systems might trigger the triboelectric effect and generate triboelectric voltages to offset the proposed output voltage. Advanced computational modelling may serve as an efficient and cost-effective method to prevent or mitigate these issues by simulating the distributions of mechanical, thermal, and solar fields within the hybrid system and designing smart architecture [251].

(3) **Self-healing.** The current self-healing mechanisms are understood by theories of bonds or protons interactions, or dipole charges attractions. However, these do not provide foundations to understand the important healing precision, healing speed, and recovery degree. Advanced microscopies [252] may underpin the mechanisms of healing precision and speed by providing atomic-level insights during healing processes. Additionally, more self-healing piezoelectric crystals are expected to be discovered due to their advantages of high piezoelectric output and high healing precision. Data mining may play a crucial role in this aspect to identify potential candidates with non-centrosymmetric space groups and dispersive functional groups from the crystallographic database following crystal engineering principles.

(4) **Biodegradability.** Although biodegradability may not be deemed as an expedient secondary function for piezoelectric biomedical energy harvesting due to the concern of unpredictable or hard-to-control premature function failure during the advance of *in vivo* biodegradation, biodegradable piezoelectric implants are very promising for applications of transient sensors and transducers. In addition to improving piezoelectric responses, the challenges to develop biodegradable piezoelectric implants lie in (i) the numerous metastable polymorphs of biodegradable polymers with strong piezoelectricity (e.g., β-glycine), and (ii) the complicated and unpredictable physiological environments and the cell's inflammatory responses. More long-term *in vivo* biodegradability studies using various (large) animal models or clinical studies should be conducted in the future, in conjunction with the latest understanding of physiological environments and inflammatory responses in biomedical science [253]. This will help to ascertain the *in vivo* biodegradation processes, stability, and durability of biodegradable piezoelectric implants, providing feedback for the optimisations of materials engineering.

Declaration of competing interest

The authors declare that they have no known competing financial interests or personal relationships that could have appeared to influence

the work reported in this paper.

Acknowledgements

The authors acknowledge the support of the Australian Research Council through the ARC Research Hub for Advanced Manufacturing of Medical Devices (IH150100024). Y. Wang truly appreciate the confidence and support from M.Y. Kong, Happy Birthday.

Received: ((will be filled in by the editorial staff))Revised: ((will be filled in by the editorial staff)) Published online: ((will be filled in by the editorial sta ff))

References

[1] M. Shirvanimoghaddam, K. Shirvanimoghaddam, M.M. Abolhasani, M. Farhangi, V. Zahiri Barsari, H. Liu, M. Dohler, M. Naebe, Towards a green and self-powered internet of Things using piezoelectric energy harvesting, IEEE Access 7 (2019) 94533–94556.
[2] M.T. Chorsi, E.J. Curry, H.T. Chorsi, R. Das, J. Baroody, P.K. Purohit, H. Ilies, T. D. Nguyen, Piezoelectric biomaterials for sensors and actuators, Adv. Mater. 31 (1) (2019), e1802084.
[3] Z.L. Wang, J. Song, Piezoelectric nanogenerators based on zinc oxide nanowire arrays, Science 312 (5771) (2006) 242.
[4] L. Lu, W. Ding, J. Liu, B. Yang, Flexible PVDF based piezoelectric nanogenerators, Nano Energy 78 (2020), 105251.
[5] R. Jayashree, Global Piezoelectric Devices Market, 2019.
[6] X. Chen, K. Parida, J. Wang, J. Xiong, M.F. Lin, J. Shao, P.S. Lee, A stretchable and transparent nanocomposite nanogenerator for self-powered physiological monitoring, ACS Appl. Mater. Interfaces 9 (48) (2017) 42200–42209.
[7] Y. Cha, J. Seo, J.-S. Kim, J.-M. Park, Human–computer interface glove using flexible piezoelectric sensors, Smart Mater. Struct. 26 (5) (2017), 057002.
[8] E.J. Lee, T.Y. Kim, S.-W. Kim, S. Jeong, Y. Choi, S.Y. Lee, High-performance piezoelectric nanogenerators based on chemically-reinforced composites, Energy Environ. Sci. 11 (6) (2018) 1425–1430.
[9] T. Ha, J. Tran, S. Liu, H. Jang, H. Jeong, R. Mitbander, H. Huh, Y. Qiu, J. Duong, R.L. Wang, P. Wang, A. Tandon, J. Sirohi, N. Lu, A chest-laminated ultrathin and stretchable E-tattoo for the measurement of electrocardiogram, seismocardiogram, and cardiac time intervals, Adv. Sci. 6 (14) (2019), 1900290.
[10] Y.-K. Fuh, P.-C. Chen, Z.-M. Huang, H.-C. Ho, Self-powered sensing elements based on direct-write, highly flexible piezoelectric polymeric nano/microfibers, Nano Energy 11 (2015) 671–677.
[11] I. Choudhry, H.R. Khalid, H.-K. Lee, Flexible piezoelectric transducers for energy harvesting and sensing from human kinematics, ACS Appl. Electron. Mater. 2 (10) (2020) 3346–3357.
[12] E.J. Curry, T.T. Le, R. Das, K. Ke, E.M. Santorella, D. Paul, M.T. Chorsi, K.T. M. Tran, J. Baroody, E.R. Borges, B. Ko, A. Golabchi, X. Xin, D. Rowe, L. Yue, J. Feng, M.D. Morales-Acosta, Q. Wu, I.P. Chen, X.T. Cui, J. Pachter, T.D. Nguyen, Biodegradable nanofiber-based piezoelectric transducer, Proc. Natl. Acad. Sci. U. S.A. 117 (1) (2020) 214–220.
[13] R. Das, E.J. Curry, T.T. Le, G. Awale, Y. Liu, S. Li, J. Contreras, C. Bednarz, J. Millender, X. Xin, D. Rowe, S. Emadi, K.W.H. Lo, T.D. Nguyen, Biodegradable nanofiber bone-tissue scaffold as remotely-controlled and self-powering electrical stimulator, Nano Energy 76 (2020).
[14] H. Zhang, X.-S. Zhang, X. Cheng, Y. Liu, M. Han, X. Xue, S. Wang, F. Yang, S. A S, H. Zhang, Z. Xu, A flexible and implantable piezoelectric generator harvesting energy from the pulsation of ascending aorta: in vitro and in vivo studies, Nano Energy 12 (2015) 296–304.
[15] S. Azimi, A. Golabchi, A. Nekookar, S. Rabbani, M.H. Amiri, K. Asadi, M. M. Abolhasani, Self-powered cardiac pacemaker by piezoelectric polymer nanogenerator implant, Nano Energy 83 (2021).
[16] E.J. Curry, K. Ke, M.T. Chorsi, K.S. Wrobel, A.N. Miller 3rd, A. Patel, I. Kim, J. Feng, L. Yue, Q. Wu, C.L. Kuo, K.W. Lo, C.T. Laurencin, H. Ilies, P.K. Purohit, T. D. Nguyen, Biodegradable piezoelectric force sensor, Proc. Natl. Acad. Sci. U.S.A. 115 (5) (2018) 909–914.
[17] D.K. Piech, B.C. Johnson, K. Shen, M.M. Ghanbari, K.Y. Li, R.M. Neely, J.E. Kay, J. M. Carmena, M.M. Maharbiz, R. Muller, A wireless millimetre-scale implantable neural stimulator with ultrasonically powered bidirectional communication, Nat. Biomed. Eng. 4 (2) (2020) 207–222.
[18] T. Inaoka, H. Shintaku, T. Nakagawa, S. Kawano, H. Ogita, T. Sakamoto, S. Hamanishi, H. Wada, J. Ito, Piezoelectric materials mimic the function of the cochlear sensory epithelium, Proc. Natl. Acad. Sci. USA 108 (45) (2011), 18390.
[19] T. Sun, J. Wright, T. Datta-Chaudhuri, Ultrasound powered piezoelectric neurostimulation devices: a commentary, Bioelectron. Med. 6 (1) (2020) 16.
[20] Z. Huo, X. Wang, Y. Zhang, B. Wan, W. Wu, J. Xi, Z. Yang, G. Hu, X. Li, C. Pan, High-performance Sb-doped p-ZnO NW films for self-powered piezoelectric strain sensors, Nano Energy 73 (2020).
[21] J.H. Kang, D.K. Jeong, S.W. Ryu, Transparent, flexible piezoelectric nanogenerator based on GaN membrane using electrochemical lift-off, ACS Appl. Mater. Interfaces 9 (12) (2017) 10637–10642.
[22] C.-T. Huang, J. Song, W.-F. Lee, Y. Ding, Z. Gao, Y. Hao, L.-J. Chen, Z.L. Wang, GaN nanowire arrays for high-output nanogenerators, J. Am. Chem. Soc. 132 (13) (2010) 4766–4771.
[23] Y.-F. Lin, J. Song, Y. Ding, S.-Y. Lu, Z.L. Wang, Piezoelectric nanogenerator using CdS nanowires, Appl. Phys. Lett. 92 (2) (2008).
[24] C.T. Huang, J. Song, C.M. Tsai, W.F. Lee, D.H. Lien, Z. Gao, Y. Hao, L.J. Chen, Z. L. Wang, Single-InN-nanowire nanogenerator with upto 1 V output voltage, Adv. Mater. 22 (36) (2010) 4008–4013.
[25] M.-Y. Lu, J. Song, M.-P. Lu, C.-Y. Lee, L.-J. Chen, Z.L. Wang, ZnO−ZnS heterojunction and ZnS nanowire arrays for electricity generation, ACS Nano 3 (2) (2009) 357–362.
[26] K.I. Park, J.H. Son, G.T. Hwang, C.K. Jeong, J. Ryu, M. Koo, I. Choi, S.H. Lee, M. Byun, Z.L. Wang, K.J. Lee, Highly-efficient, flexible piezoelectric PZT thin film nanogenerator on plastic substrates, Adv. Mater. 26 (16) (2014) 2514–2520.
[27] K. Wieczorek, A. Ziebiniska, Z. Ujma, K. Szot, M. Górny, I. Franke, J. Koperski, A. Soszyński, K. Roleder, Electrostrictive and piezoelectric effect in BaTiO3 and PbZrO3, Ferroelectrics 336 (1) (2006) 61–67.
[28] S. Zhang, F. Li, X. Jiang, J. Kim, J. Luo, X. Geng, Advantages and challenges of relaxor-PbTiO3 ferroelectric crystals for electroacoustic transducers – a review, Prog. Mater. Sci. 68 (2015) 1–66.
[29] M. Acosta, N. Novak, V. Rojas, S. Patel, R. Vaish, J. Koruza, G.A. Rossetti, J. Rödel, BaTiO3-based piezoelectrics: fundamentals, current status, and perspectives, Appl. Phys. Rev. 4 (4) (2017), 041305.
[30] M. Xu, H. Kang, L. Guan, H. Li, M. Zhang, Facile fabrication of a flexible LiNbO3 piezoelectric sensor through hot pressing for biomechanical monitoring, ACS Appl. Mater. Interfaces 9 (40) (2017) 34687–34695.
[31] T. Zheng, H. Wu, Y. Yuan, X. Lv, Q. Li, T. Men, C. Zhao, D. Xiao, J. Wu, K. Wang, J.-F. Li, Y. Gu, J. Zhu, S.J. Pennycook, The structural origin of enhanced piezoelectric performance and stability in lead free ceramics, Energy Environ. Sci. 10 (2) (2017) 528–537.
[32] A. Verma, N. Panayanthatta, A. Ichangi, T. Fischer, L. Montes, E. Bano, S. Mathur, Interdependence of piezoelectric coefficient and film thickness in LiTaO3 cantilevers, J. Am. Ceram. Soc. 104 (5) (2021) 1966–1977.
[33] T. Huang, C. Wang, H. Yu, H. Wang, Q. Zhang, M. Zhu, Human walking-driven wearable all-fiber triboelectric nanogenerator containing electrospun polyvinylidene fluoride piezoelectric nanofibers, Nano Energy 14 (2015) 226–235.
[34] Y. Li, M.-H. Xu, Y.-S. Xia, J.-M. Wu, X.-K. Sun, S. Wang, G.-H. Hu, C.-X. Xiong, Multilayer assembly of electrospun/electrosprayed PVDF-based nanofibers and beads with enhanced piezoelectricity and high sensitivity, Chem. Eng. J. 388 (2020), 124205.
[35] T. Sharma, S.-S. Je, B. Gill, J.X.J. Zhang, Patterning piezoelectric thin film PVDF–TrFE based pressure sensor for catheter application, Sensor Actuator Phys. 177 (2012) 87–92.
[36] S. Anwar, M. Hassanpour Amiri, S. Jiang, M.M. Abolhasani, P.R.F. Rocha, K. Asadi, Piezoelectric nylon-11 fibers for electronic textiles, energy harvesting and sensing, Adv. Funct. Mater. 31 (4) (2021), 2004326.
[37] T. Zheng, Z. Yue, G.G. Wallace, Y. Du, M.J. Higgins, Nanoscale piezoelectric effect of biodegradable PLA-based composite fibers by piezoresponse force microscopy, Nanotechnology 31 (37) (2020), 375708.
[38] A. Sultana, S.K. Ghosh, V. Sencadas, T. Zheng, M.J. Higgins, T.R. Middya, D. Mandal, Human skin interactive self-powered wearable piezoelectric bio-e-skin by electrospun poly-l-lactic acid nanofibers for non-invasive physiological signal monitoring, J. Mater. Chem. B 5 (35) (2017) 7352–7359.
[39] M. Yoshida, T. Onogi, K. Onishi, T. Inagaki, Y. Tajitsu, High piezoelectric performance of poly(lactic acid) film manufactured by solid-state extrusion, Jpn. J. Appl. Phys. 53 (9S) (2014), 09PC02.
[40] V.V. Lemanov, S.N. Popov, G.A. Pankova, Piezoelectricity in protein amino acids, Phys. Solid State 53 (6) (2011) 1191–1193.
[41] S. Bera, S. Guerin, H. Yuan, J. O'Donnell, N.P. Reynolds, O. Maraba, W. Ji, L.J. W. Shimon, P.A. Cazade, S.A.M. Tofail, D. Thompson, R. Yang, E. Gazit, Molecular engineering of piezoelectricity in collagen-mimicking peptide assemblies, Nat. Commun. 12 (1) (2021) 2634.
[42] E. Fukada, I. Yasuda, Piezoelectric effects in collagen, Jpn. J. Appl. Phys. 3 (2) (1964) 117–121.
[43] B.Y. Lee, J. Zhang, C. Zueger, W.J. Chung, S.Y. Yoo, E. Wang, J. Meyer, R. Ramesh, S.W. Lee, Virus-based piezoelectric energy generation, Nat. Nanotechnol. 7 (6) (2012) 351–356.
[44] D.-M. Shin, H.J. Han, W.-G. Kim, E. Kim, C. Kim, S.W. Hong, H.K. Kim, J.-W. Oh, Y.-H. Hwang, Bioinspired piezoelectric nanogenerators based on vertically aligned phage nanopillars, Energy Environ. Sci. 8 (11) (2015) 3198–3203.
[45] H.-Y. Ye, Y.-Y. Tang, P.-F. Li, W.-Q. Liao, J.-X. Gao, X.-N. Hua, H. Cai, P.-P. Shi, Y.-M. You, R.-G. Xiong, Metal-free three-dimensional perovskite ferroelectrics, Science 361 (6398) (2018) 151–155.
[46] D. Ponnamma, M. Al Ali Al-Maadeed, Influence of BaTiO3/white graphene filler synergy on the energy harvesting performance of a piezoelectric polymer nanocomposite, Sustain. Energy Fuels 3 (3) (2019) 774–785.
[47] D. Singh, A. Choudhary, A. Garg, Flexible and robust piezoelectric polymer nanocomposites based energy harvesters, ACS Appl. Mater. Interfaces 10 (3) (2018) 2793–2800.
[48] B. Dudem, D.H. Kim, L.K. Bharat, J.S. Yu, Highly-flexible piezoelectric nanogenerators with silver nanowires and barium titanate embedded composite films for mechanical energy harvesting, Appl. Energy 230 (2018) 865–874.
[49] A. Jain, P. K. J, A.K. Sharma, A. Jain, R. P.N, Dielectric and piezoelectric properties of PVDF/PZT composites: a review, Polym. Eng. Sci. 55 (7) (2015) 1589–1616.
[50] Y. Zhang, L. Chen, J. Zeng, K. Zhou, D. Zhang, Aligned porous barium titanate/hydroxyapatite composites with high piezoelectric coefficients for bone tissue engineering, Mater. Sci. Eng. C 39 (2014) 143–149.

[51] M. Xia, C. Luo, X. Su, Y. Li, P. Li, J. Hu, G. Li, H. Jiang, W. Zhang, KNN/PDMS/C-based lead-free piezoelectric composite film for flexible nanogenerator, J. Mater. Sci. Mater. Electron. 30 (8) (2019) 7558–7566.

[52] V. Cauda, S. Stassi, A. Lamberti, M. Morello, C. Fabrizio Pirri, G. Canavese, Leveraging ZnO morphologies in piezoelectric composites for mechanical energy harvesting, Nano Energy 18 (2015) 212–221.

[53] A. Das, D. Pamu, A comprehensive review on electrical properties of hydroxyapatite based ceramic composites, Mater. Sci. Eng. C 101 (2019) 539–563.

[54] P. Li, J. Zhai, B. Shen, S. Zhang, X. Li, F. Zhu, X. Zhang, Ultrahigh piezoelectric properties in textured (K,Na)NbO3-based lead-free ceramics, Adv. Mater. 30 (8) (2018), 1705171.

[55] T. Kimura, Application of texture engineering to piezoelectric ceramics: a review, J. Ceram. Soc. Jpn. 114 (1325) (2006) 15–25.

[56] N.A. Shepelin, P.C. Sherrell, E. Goudeli, E.N. Skountzos, V.C. Lussini, G. W. Dicinoski, J.G. Shapter, A.V. Ellis, Printed recyclable and self-poled polymer piezoelectric generators through single-walled carbon nanotube templating, Energy Environ. Sci. 13 (3) (2020) 868–883.

[57] L. Persano, C. Dagdeviren, Y. Su, Y. Zhang, S. Girardo, D. Pisignano, Y. Huang, J. A. Rogers, High performance piezoelectric devices based on aligned arrays of nanofibers of poly(vinylidenefluoride-co-trifluoroethylene), Nat. Commun. 4 (1) (2013) 1633.

[58] N.A. Shepelin, P.C. Sherrell, E.N. Skountzos, E. Goudeli, J. Zhang, V.C. Lussini, B. Imtiaz, K.A.S. Usman, G.W. Dicinoski, J.G. Shapter, J.M. Razal, A.V. Ellis, Interfacial piezoelectric polarization locking in printable Ti3C2Tx MXene-fluoropolymer composites, Nat. Commun. 12 (1) (2021) 3171.

[59] J.I. Sohn, S.N. Cha, B.G. Song, S. Lee, S.M. Kim, J. Ku, H.J. Kim, Y.J. Park, B. L. Choi, Z.L. Wang, J.M. Kim, K. Kim, Engineering of efficiency limiting free carriers and an interfacial energy barrier for an enhancing piezoelectric generation, Energy Environ. Sci. 6 (1) (2013) 97–104.

[60] P. Adhikary, S. Garain, S. Ram, D. Mandal, Flexible hybrid eu3+ doped P(VDF-HFP) nanocomposite film possess hypersensitive electronic transitions and piezoelectric throughput, J. Polym. Sci. B Polym. Phys. 54 (22) (2016) 2335–2345.

[61] X. Gao, Z. Cheng, Z. Chen, Y. Liu, X. Meng, X. Zhang, J. Wang, Q. Guo, B. Li, H. Sun, Q. Gu, H. Hao, Q. Shen, J. Wu, X. Liao, S.P. Ringer, H. Liu, L. Zhang, W. Chen, F. Li, S. Zhang, The mechanism for the enhanced piezoelectricity in multi-elements doped (K,Na)NbO3 ceramics, Nat. Commun. 12 (1) (2021) 881.

[62] X. Chen, X. Li, J. Shao, N. An, H. Tian, C. Wang, T. Han, L. Wang, B. Lu, High-performance piezoelectric nanogenerators with imprinted P(VDF-TrFE)/$BaTiO_3$ nanocomposite micropillars for self-powered flexible sensors, Small 13 (23) (2017).

[63] G.F. Yu, X. Yan, M. Yu, M.Y. Jia, W. Pan, X.X. He, W.P. Han, Z.M. Zhang, L.M. Yu, Y.Z. Long, Patterned, highly stretchable and conductive nanofibrous PANI/PVDF strain sensors based on electrospinning and in situ polymerization, Nanoscale 8 (5) (2016) 2944–2950.

[64] J. Park, M. Kim, Y. Lee, H.S. Lee, H. Ko, Fingertip skin-inspired microstructured ferroelectric skins discriminate static/dynamic pressure and temperature stimuli, Sci. Adv. 1 (9) (2015), e1500661.

[65] X. Chen, X. Li, J. Shao, N. An, H. Tian, C. Wang, T. Han, L. Wang, B. Lu, High-performance piezoelectric nanogenerators with imprinted P(VDF-TrFE)/BaTiO3 nanocomposite micropillars for self-powered flexible sensors, Small 13 (23) (2017), 1604245.

[66] C. Shuai, G. Liu, Y. Yang, F. Qi, S. Peng, W. Yang, C. He, G. Wang, G. Qian, A strawberry-like Ag-decorated barium titanate enhances piezoelectric and antibacterial activities of polymer scaffold, Nano Energy 74 (2020), 104825.

[67] J. Wang, S. Zhou, Z. Zhang, D. Yurchenko, High-performance piezoelectric wind energy harvester with Y-shaped attachments, Energy Convers. Manag. 181 (2019) 645–652.

[68] N. Sezer, M. Koç, A comprehensive review on the state-of-the-art of piezoelectric energy harvesting, Nano Energy 80 (2021).

[69] Z.L. Wang, Nanopiezotronics, Adv. Mater. 19 (6) (2007) 889–892.

[70] W.-S. Jung, M.-J. Lee, M.-G. Kang, H.G. Moon, S.-J. Yoon, S.-H. Baek, C.-Y. Kang, Powerful curved piezoelectric generator for wearable applications, Nano Energy 13 (2015) 174–181.

[71] H. Zhou, Y. Zhang, Y. Qiu, H. Wu, W. Qin, Y. Liao, Q. Yu, H. Cheng, Stretchable piezoelectric energy harvesters and self-powered sensors for wearable and implantable devices, Biosens. Bioelectron. 168 (2020), 112569.

[72] K.-I. Park, C.K. Jeong, N.K. Kim, K.J. Lee, Stretchable piezoelectric nanocomposite generator, Nano Convergence 3 (1) (2016) 12.

[73] F. Ali, W. Raza, X. Li, H. Gul, K.-H. Kim, Piezoelectric energy harvesters for biomedical applications, Nano Energy 57 (2019) 879–902.

[74] Z. Li, Q. Zheng, Z.L. Wang, Z. Li, Nanogenerator-based self-powered sensors for wearable and implantable electronics, Research 2020 (2020), 8710686.

[75] C.K. Jeong, Toward bioimplantable and biocompatible flexible energy harvesters using piezoelectric ceramic materials, MRS Communications 10 (3) (2020) 365–378.

[76] J. Li, T.A. Hacker, H. Wei, Y. Long, F. Yang, D. Ni, A. Rodgers, W. Cai, X. Wang, Long-term in vivo operation of implanted cardiac nanogenerators in swine, Nano Energy 90 (2021), 106507.

[77] C.K. Jeong, J. Lee, S. Han, J. Ryu, G.T. Hwang, D.Y. Park, J.H. Park, S.S. Lee, M. Byun, S.H. Ko, K.J. Lee, A hyper-stretchable elastic-composite energy harvester, Adv. Mater. 27 (18) (2015) 2866–2875.

[78] C. Hu, K. Behdinan, R. Moradi-Dastjerdi, PVDF energy harvester for prolonging the battery life of cardiac pacemakers, Actuators 11 (7) (2022) 187.

[79] J. Zhang, D. Liu, Q. Han, L. Jiang, H. Shao, B. Tang, W. Lei, T. Lin, C.H. Wang, Mechanically stretchable piezoelectric polyvinylidene fluoride (PVDF)/Boron nitride nanosheets (BNNSs) polymer nanocomposites, Compos. B Eng. 175 (2019), 107157.

[80] S. Siddiqui, H.B. Lee, D.-I. Kim, L.T. Duy, A. Hanif, N.-E. Lee, An omnidirectionally stretchable piezoelectric nanogenerator based on hybrid nanofibers and carbon electrodes for multimodal straining and human kinematics energy harvesting, Adv. Energy Mater. 8 (2) (2018), 1701520.

[81] S.-R. Kim, J.-H. Yoo, Y.S. Cho, J.-W. Park, Flexible piezoelectric energy generators based on P(VDF-TrFE) nanofibers, Mater. Res. Express 6 (8) (2019), 086311.

[82] K.-I. Park, J.H. Son, G.-T. Hwang, C.K. Jeong, J. Ryu, M. Koo, I. Choi, S.H. Lee, M. Byun, Z.L. Wang, K.J. Lee, Highly-efficient, flexible piezoelectric PZT thin film nanogenerator on plastic substrates, Adv. Mater. 26 (16) (2014) 2514–2520.

[83] J. Seo, Y. Kim, W.Y. Park, J.Y. Son, C.K. Jeong, H. Kim, W.-H. Kim, Out-of-plane piezoresponse of monolayer MoS2 on plastic substrates enabled by highly uniform and layer-controllable CVD, Appl. Surf. Sci. 487 (2019) 1356–1361.

[84] C. Dagdeviren, B.D. Yang, Y. Su, P.L. Tran, P. Joe, E. Anderson, J. Xia, V. Doraiswamy, B. Dehdashti, X. Feng, B. Lu, R. Poston, Z. Khalpey, R. Ghaffari, Y. Huang, M.J. Slepian, J.A. Rogers, Conformal piezoelectric energy harvesting and storage from motions of the heart, lung, and diaphragm, Proc. Natl. Acad. Sci. USA 111 (5) (2014) 1927–1932.

[85] H.G. Yeo, T. Xue, S. Roundy, X. Ma, C. Rahn, S. Trolier-McKinstry, Strongly (001) oriented bimorph PZT film on metal foils grown by rf-sputtering for wrist-worn piezoelectric energy harvesters, Adv. Funct. Mater. 28 (36) (2018), 1801327.

[86] K. Shibata, F. Oka, A. Ohishi, T. Mishima, I. Kanno, Piezoelectric properties of (K, Na)NbO_3Films deposited by RF magnetron sputtering, APEX 1 (1) (2008), 011501.

[87] Y.J. Ko, D.Y. Kim, S.S. Won, C.W. Ahn, I.W. Kim, A.I. Kingon, S.-H. Kim, J.-H. Ko, J.H. Jung, Flexible $Pb(Zr_{0.52}Ti_{0.48})O_3$ films for a hybrid piezoelectric-pyroelectric nanogenerator under harsh environments, ACS Appl. Mater. Interfaces 8 (10) (2016) 6504–6511.

[88] H.G. Yeo, J. Jung, M. Sim, J.E. Jang, H. Choi, Integrated piezoelectric AlN thin film with SU-8/PDMS supporting layer for flexible sensor array, Sensors 20 (1) (2020) 315.

[89] J. Li, L. Kang, Y. Yu, Y. Long, J.J. Jeffery, W. Cai, X. Wang, Study of long-term biocompatibility and bio-safety of implantable nanogenerators, Nano Energy 51 (2018) 728–735.

[90] C.K. Jeong, J.H. Han, H. Palneedi, H. Park, G.-T. Hwang, B. Joung, S.-G. Kim, H. J. Shin, I.-S. Kang, J. Ryu, K.J. Lee, Comprehensive biocompatibility of nontoxic and high-output flexible energy harvester using lead-free piezoceramic thin film, Apl. Mater. 5 (7) (2017), 074102.

[91] Y. Zhang, H. Kim, Q. Wang, W. Jo, A.I. Kingon, S.-H. Kim, C.K. Jeong, Progress in lead-free piezoelectric nanofiller materials and related composite nanogenerator devices, Nanoscale Adv. 2 (8) (2020) 3131–3149.

[92] D.H. Kim, H.J. Shin, H. Lee, C.K. Jeong, H. Park, G.-T. Hwang, H.-Y. Lee, D.J. Joe, J.H. Han, S.H. Lee, J. Kim, B. Joung, K.J. Lee, In vivo self-powered wireless transmission using biocompatible flexible energy harvesters, Adv. Funct. Mater. 27 (25) (2017), 1700341.

[93] J. Curie, P. Curie, Development, via compression, of electric polarization in hemihedral crystals with inclined faces, Bull. Soc. Min. Fr. 3 (1880) 90–93.

[94] G. Lippman, Principal of the conservation of electricity, Ann. Chem. Phys. 24 (1881) 145.

[95] T.R. Shrout, S.J. Zhang, Lead-free piezoelectric ceramics: alternatives for PZT? J. Electroceram. 19 (1) (2007) 113–126.

[96] Y.Q. Fu, J.K. Luo, N.T. Nguyen, A.J. Walton, A.J. Flewitt, X.T. Zu, Y. Li, G. McHale, A. Matthews, E. Iborra, H. Du, W.I. Milne, Advances in piezoelectric thin films for acoustic biosensors, acoustofluidics and lab-on-chip applications, Prog. Mater. Sci. 89 (2017) 31–91.

[97] W. Wu, Z.L. Wang, Piezotronics and piezo-phototronics for adaptive electronics and optoelectronics, Nat. Rev. Mater. 1 (7) (2016), 16031.

[98] S.B. Lang, S.A.M. Tofail, A.L. Kholkin, M. Wojtaś, M. Gregor, A.A. Gandhi, Y. Wang, S. Bauer, M. Krause, A. Plecenik, Ferroelectric polarization in nanocrystalline hydroxyapatite thin films on silicon, Sci. Rep. 3 (2013) 2215, 2215.

[99] D.M. Shin, S.W. Hong, Y.H. Hwang, Recent advances in organic piezoelectric biomaterials for energy and biomedical applications, Nanomaterials 10 (1) (2020).

[100] Q. Li, Q. Wang, Ferroelectric polymers and their energy-related applications, Macromol. Chem. Phys. 217 (11) (2016) 1228–1244.

[101] G.H. Haertling, Ferroelectric ceramics: history and technology, J. Am. Ceram. Soc. 82 (4) (1999) 797–818.

[102] Y. Qi, J. Kim, T.D. Nguyen, B. Lisko, P.K. Purohit, M.C. McAlpine, Enhanced piezoelectricity and stretchability in energy harvesting devices fabricated from buckled PZT ribbons, Nano Lett. 11 (3) (2011) 1331–1336.

[103] X. Feng, B.D. Yang, Y. Liu, Y. Wang, C. Dagdeviren, Z. Liu, A. Carlson, J. Li, Y. Huang, J.A. Rogers, Stretchable ferroelectric nanoribbons with wavy configurations on elastomeric substrates, ACS Nano 5 (4) (2011) 3326–3332.

[104] S. Xu, B.J. Hansen, Z.L. Wang, Piezoelectric-nanowire-enabled power source for driving wireless microelectronics, Nat. Commun. 1 (1) (2010) 93.

[105] R.N. Torah, S.P. Beeby, N.M. White, Experimental investigation into the effect of substrate clamping on the piezoelectric behaviour of thick-film PZT elements, J. Phys. Appl. Phys. 37 (7) (2004) 1074–1078.

[106] Y. Su, S. Li, R. Li, C. Dagdeviren, Splitting of neutral mechanical plane of conformal, multilayer piezoelectric mechanical energy harvester, Appl. Phys. Lett. 107 (4) (2015), 041905.

[107] Y. Zhang, F. Zhang, Z. Yan, Q. Ma, X. Li, Y. Huang, J.A. Rogers, Printing, folding and assembly methods for forming 3D mesostructures in advanced materials, Nat. Rev. Mater. 2 (4) (2017), 17019.
[108] S. Xu, Z. Yan, K.-I. Jang, W. Huang, H. Fu, J. Kim, Z. Wei, M. Flavin, J. McCracken, R. Wang, A. Badea, Y. Liu, D. Xiao, G. Zhou, J. Lee, H.U. Chung, H. Cheng, W. Ren, A. Banks, X. Li, U. Paik, R.G. Nuzzo, Y. Huang, Y. Zhang, J. A. Rogers, Assembly of micro/nanomaterials into complex, three-dimensional architectures by compressive buckling, Science 347 (6218) (2015) 154–159.
[109] M. Han, H. Wang, Y. Yang, C. Liang, W. Bai, Z. Yan, H. Li, Y. Xue, X. Wang, B. Akar, H. Zhao, H. Luan, J. Lim, I. Kandela, G.A. Ameer, Y. Zhang, Y. Huang, J. A. Rogers, Three-dimensional piezoelectric polymer microsystems for vibrational energy harvesting, robotic interfaces and biomedical implants, Nature Electronics 2 (1) (2019) 26–35.
[110] X. Zhou, K. Parida, O. Halevi, Y. Liu, J. Xiong, S. Magdassi, P.S. Lee, All 3D-printed stretchable piezoelectric nanogenerator with non-protruding kirigami structure, Nano Energy 72 (2020).
[111] Y. Duan, Y. Huang, Z. Yin, N. Bu, W. Dong, Non-wrinkled, highly stretchable piezoelectric devices by electrohydrodynamic direct-writing, Nanoscale 6 (6) (2014) 3289–3295.
[112] Y. Ding, Y. Duan, Y. Huang, Electrohydrodynamically printed, flexible energy harvester using in situ poled piezoelectric nanofibers, Energy Technol. 3 (4) (2015) 351–358.
[113] Y. Duan, Y. Ding, J. Bian, Z. Xu, Z. Yin, Y. Huang, Ultra-stretchable piezoelectric nanogenerators via large-scale Aligned fractal inspired micro/nanofibers, Polymers 9 (12) (2017).
[114] Y. Huang, Y. Ding, J. Bian, Y. Su, J. Zhou, Y. Duan, Z. Yin, Hyper-stretchable self-powered sensors based on electrohydrodynamically printed, self-similar piezoelectric nano/microfibers, Nano Energy 40 (2017) 432–439.
[115] J.H. Lee, K.Y. Lee, M.K. Gupta, T.Y. Kim, D.Y. Lee, J. Oh, C. Ryu, W.J. Yoo, C. Y. Kang, S.J. Yoon, J.B. Yoo, S.W. Kim, Highly stretchable piezoelectric-pyroelectric hybrid nanogenerator, Adv. Mater. 26 (5) (2014) 765–769.
[116] Y. Mao, P. Zhao, G. McConohy, H. Yang, Y. Tong, X. Wang, Sponge-like piezoelectric polymer films for scalable and integratable nanogenerators and self-powered electronic systems, Adv. Energy Mater. 4 (7) (2014), 1301624.
[117] F. Mokhtari, G.M. Spinks, S. Sayyar, Z. Cheng, A. Ruhparwar, J. Foroughi, Highly stretchable self-powered wearable electrical energy generator and sensors, Adv. Mater. Technol 6 (2) (2020).
[118] M. Baniasadi, J. Huang, Z. Xu, S. Moreno, X. Yang, J. Chang, M.A. Quevedo-Lopez, M. Naraghi, M. Minary-Jolandan, High-performance coils and yarns of polymeric piezoelectric nanofibers, ACS Appl. Mater. Interfaces 7 (9) (2015) 5358–5366.
[119] H.J. Sim, C. Choi, C.J. Lee, Y.T. Kim, G.M. Spinks, M.D. Lima, R.H. Baughman, S. J. Kim, Flexible, stretchable and weavable piezoelectric fiber, Adv. Eng. Mater. 17 (9) (2015) 1270–1275.
[120] S.K. Karan, D. Mandal, B.B. Khatua, Self-powered flexible Fe-doped RGO/PVDF nanocomposite: an excellent material for a piezoelectric energy harvester, Nanoscale 7 (24) (2015) 10655–10666.
[121] D. Yun, K.S. Yun, Woven piezoelectric structure for stretchable energy harvester, Electron. Lett. 49 (1) (2013) 65–66.
[122] Y. Ahn, S. Song, K.-S. Yun, Woven flexible textile structure for wearable power-generating tactile sensor array, Smart Mater. Struct. 24 (7) (2015), 075002.
[123] M. Kim, K.-S. Yun, Helical piezoelectric energy harvester and its application to energy harvesting garments, Micromachines 8 (4) (2017) 115.
[124] M. Zhang, T. Gao, J. Wang, J. Liao, Y. Qiu, Q. Yang, H. Xue, Z. Shi, Y. Zhao, Z. Xiong, L. Chen, A hybrid fibers based wearable fabric piezoelectric nanogenerator for energy harvesting application, Nano Energy 13 (2015) 298–305.
[125] K. Dong, X. Peng, Z.L. Wang, Fiber/fabric-based piezoelectric and triboelectric nanogenerators for flexible/stretchable and wearable electronics and artificial intelligence, Adv. Mater. 32 (5) (2020), e1902549.
[126] A. Lund, K. Rundqvist, E. Nilsson, L. Yu, B. Hagström, C. Müller, Energy harvesting textiles for a rainy day: woven piezoelectrics based on melt-spun PVDF microfibres with a conducting core, npj Flexible Electronics 2 (1) (2018).
[127] S. Lim, D. Son, J. Kim, Y.B. Lee, J.-K. Song, S. Choi, D.J. Lee, J.H. Kim, M. Lee, T. Hyeon, D.-H. Kim, Transparent and stretchable interactive human machine interface based on patterned graphene heterostructures, Adv. Funct. Mater. 25 (3) (2015) 375–383.
[128] Z. Song, X. Wang, C. Lv, Y. An, M. Liang, T. Ma, D. He, Y.-J. Zheng, S.-Q. Huang, H. Yu, H. Jiang, Kirigami-based stretchable lithium-ion batteries, Sci. Rep. 5 (1) (2015), 10988.
[129] M. Eidini, G.H. Paulino, Unraveling metamaterial properties in zigzag-base folded sheets, Sci. Adv. 1 (8) (2015), e1500224.
[130] A. Lamoureux, K. Lee, M. Shlian, S.R. Forrest, M. Shtein, Dynamic kirigami structures for integrated solar tracking, Nat. Commun. 6 (1) (2015) 8092.
[131] N. Hu, D. Chen, D. Wang, S. Huang, I. Trase, H.M. Grover, X. Yu, J.X.J. Zhang, Z. Chen, Stretchable kirigami polyvinylidene difluoride thin films for energy harvesting: design, analysis, and performance, Phys. Rev. Appl. 9 (2) (2018).
[132] R. Sun, B. Zhang, L. Yang, W. Zhang, I. Farrow, F. Scarpa, J. Rossiter, Kirigami stretchable strain sensors with enhanced piezoelectricity induced by topological electrodes, Appl. Phys. Lett. 112 (25) (2018).
[133] R.A. Surmenev, T. Orlova, R.V. Chernozem, A.A. Ivanova, A. Bartasyte, S. Mathur, M.A. Surmeneva, Hybrid lead-free polymer-based nanocomposites with improved piezoelectric response for biomedical energy-harvesting applications: a review, Nano Energy 62 (2019) 475–506.
[134] S. Das, A.K. Biswal, K. Parida, R.N.P. Choudhary, A. Roy, Electrical and mechanical behavior of PMN-PT/CNT based polymer composite film for energy harvesting, Appl. Surf. Sci. 428 (2018) 356–363.
[135] J. Ryu, J. Kim, J. Oh, S. Lim, J.Y. Sim, J.S. Jeon, K. No, S. Park, S. Hong, Intrinsically stretchable multi-functional fiber with energy harvesting and strain sensing capability, Nano Energy 55 (2019) 348–353.
[136] W. Zhai, Q. Lai, L. Chen, L. Zhu, Z.L. Wang, Flexible piezoelectric nanogenerators based on P(VDF–TrFE)/GeSe nanocomposite films, ACS Appl. Electron. Mater. 2 (8) (2020) 2369–2374.
[137] H. Parangusan, D. Ponnamma, M.A.A. Al-Maadeed, Stretchable electrospun PVDF-HFP/Co-ZnO nanofibers as piezoelectric nanogenerators, Sci. Rep. 8 (1) (2018) 754.
[138] J.E.Q. Quinsaat, T. de Wild, F.A. Nüesch, D. Damjanovic, R. Krämer, G. Schürch, D. Häfliger, F. Clemens, T. Sebastian, M. Dascalu, D.M. Opris, Stretchable piezoelectric elastic composites for sensors and energy generators, Compos. B Eng. 198 (2020), 108211.
[139] X. Chou, J. Zhu, S. Qian, X. Niu, J. Qian, X. Hou, J. Mu, W. Geng, J. Cho, J. He, C. Xue, All-in-one filler-elastomer-based high-performance stretchable piezoelectric nanogenerator for kinetic energy harvesting and self-powered motion monitoring, Nano Energy 53 (2018) 550–558.
[140] X. Niu, W. Jia, S. Qian, J. Zhu, J. Zhang, X. Hou, J. Mu, W. Geng, J. Cho, J. He, X. Chou, High-performance PZT-based stretchable piezoelectric nanogenerator, ACS Sustain. Chem. Eng. 7 (1) (2018) 979–985.
[141] H. Parangusan, D. Ponnamma, M. Al Ali AlMaadeed, Flexible tri-layer piezoelectric nanogenerator based on PVDF-HFP/Ni-doped ZnO nanocomposites, RSC Adv. 7 (79) (2017) 50156–50165.
[142] J. Li, J. Yin, C. Yang, N. Li, Y. Feng, Y. Liu, H. Zhao, Y. Li, C. Zhu, D. Yue, B. Su, X. Liu, Enhanced dielectric performance and energy storage of PVDF-HFP-based composites induced by surface charged Al2O3, J. Polym. Sci. B Polym. Phys. 57 (10) (2019) 574–583.
[143] H. Paik, Y.-Y. Choi, S. Hong, K. No, Effect of Ag nanoparticle concentration on the electrical and ferroelectric properties of Ag/P(VDF-TrFE) composite films, Sci. Rep. 5 (1) (2015), 13209.
[144] A.C. Lopes, S.A.C. Carabineiro, M.F.R. Pereira, G. Botelho, S. Lanceros-Mendez, Nanoparticle size and concentration dependence of the electroactive phase content and electrical and optical properties of Ag/Poly(vinylidene fluoride) composites, ChemPhysChem 14 (9) (2013) 1926–1933.
[145] E. Kar, N. Bose, B. Dutta, S. Banerjee, N. Mukherjee, S. Mukherjee, 2D SnO2 nanosheet/PVDF composite based flexible, self-cleaning piezoelectric energy harvester, Energy Convers. Manag. 184 (2019) 600–608.
[146] S. Song, Y. Li, Q. Wang, C. Zhang, Boosting piezoelectric performance with a new selective laser sintering 3D printable PVDF/graphene nanocomposite, Compos. Appl. Sci. Manuf. 147 (2021), 106452.
[147] D. Mandal, K. Henkel, D. Schmeisser, Control of the crystalline polymorph, molecular dipole and chain orientations in P(VDF-HFP) for high electrical energy storage application, in: 2011 International Conference on Nanoscience, Technology and Societal Implications, 2011, pp. 1–5.
[148] G. Xiong, C. Meng, R.G. Reifenberger, P.P. Irazoqui, T.S. Fisher, A review of graphene-based electrochemical microsupercapacitors, Electroanalysis 26 (1) (2014) 30–51.
[149] J. Yao, C.W.M. Bastiaansen, T. Peijs, High strength and high modulus electrospun nanofibers, Fibers 2 (2) (2014) 158–186.
[150] P. Hu, L. Yan, C. Zhao, Y. Zhang, J. Niu, Double-layer structured PVDF nanocomposite film designed for flexible nanogenerator exhibiting enhanced piezoelectric output and mechanical property, Compos. Sci. Technol. 168 (2018) 327–335.
[151] X. Yuan, X. Gao, J. Yang, X. Shen, Z. Li, S. You, Z. Wang, S. Dong, The large piezoelectricity and high power density of a 3D-printed multilayer copolymer in a rugby ball-structured mechanical energy harvester, Energy Environ. Sci. 13 (1) (2020) 152–161.
[152] J. Jiang, Z. Shen, J. Qian, Z. Dan, M. Guo, Y. He, Y. Lin, C.-W. Nan, L. Chen, Y. Shen, Synergy of micro-/mesoscopic interfaces in multilayered polymer nanocomposites induces ultrahigh energy density for capacitive energy storage, Nano Energy 62 (2019) 220–229.
[153] Y. Li, X. Su, K. Liang, C. Luo, P. Li, J. Hu, G. Li, H. Jiang, K. Wang, Multi-layered BTO/PVDF nanogenerator with highly enhanced performance induced by interlaminar electric field, Microelectron. Eng. 244–246 (2021), 111557.
[154] R.A. Surmenev, R.V. Chernozem, I.O. Pariy, M.A. Surmeneva, A review on piezo- and pyroelectric responses of flexible nano- and micropatterned polymer surfaces for biomedical sensing and energy harvesting applications, Nano Energy 79 (2021), 105442.
[155] X. Li, K. Terabe, H. Hatano, H. Zeng, K. Kitamura, Domain patterning thin crystalline ferroelectric film with focused ion beam for nonlinear photonic integrated circuits, J. Appl. Phys. 100 (10) (2006), 106103.
[156] J. Li, Y. Luo, M. Bai, S. Ducharme, Nanomesa and nanowell formation in Langmuir–Blodgett polyvinylidene fluoride trifluoroethylene copolymer films, Appl. Phys. Lett. 87 (21) (2005), 213116.
[157] Z. Hu, M. Tian, B. Nysten, A.M. Jonas, Regular arrays of highly ordered ferroelectric polymer nanostructures for non-volatile low-voltage memories, Nat. Mater. 8 (1) (2009) 62–67.
[158] H. Yang, P. Deschatelets, S.T. Brittain, G.M. Whitesides, Fabrication of high performance ceramic microstructures from a polymeric precursor using soft lithography, Adv. Mater. 13 (1) (2001) 54–58.
[159] X. Chen, H. Tian, X. Li, J. Shao, Y. Ding, N. An, Y. Zhou, A high performance P (VDF-TrFE) nanogenerator with self-connected and vertically integrated fibers by patterned EHD pulling, Nanoscale 7 (27) (2015) 11536–11544.

[160] I.O. Pariy, A.A. Ivanova, V.V. Shvartsman, D.C. Lupascu, G.B. Sukhorukov, M. A. Surmeneva, R.A. Surmenev, Poling and annealing of piezoelectric Poly (Vinylidene fluoride) micropillar arrays, Mater. Chem. Phys. 239 (2020), 122035.
[161] I.O. Pariy, A.A. Ivanova, V.V. Shvartsman, D.C. Lupascu, G.B. Sukhorukov, T. Ludwig, A. Bartasyte, S. Mathur, M.A. Surmeneva, R.A. Surmenev, Piezoelectric response in hybrid micropillar arrays of poly(vinylidene fluoride) and reduced graphene oxide, Polymers 11 (6) (2019) 1065.
[162] R.A. Whiter, V. Narayan, S. Kar-Narayan, A scalable nanogenerator based on self-poled piezoelectric polymer nanowires with high energy conversion efficiency, Adv. Energy Mater. 4 (18) (2014), 1400519.
[163] W.H. Liew, M.S. Mirshekarloo, S. Chen, K. Yao, F.E.H. Tay, Nanoconfinement induced crystal orientation and large piezoelectric coefficient in vertically aligned P(VDF-TrFE) nanotube array, Sci. Rep. 5 (1) (2015), 09790.
[164] Y. Lee, J. Park, S. Cho, Y.E. Shin, H. Lee, J. Kim, J. Myoung, S. Cho, S. Kang, C. Baig, H. Ko, Flexible ferroelectric sensors with ultrahigh pressure sensitivity and linear response over exceptionally broad pressure range, ACS Nano 12 (4) (2018) 4045–4054.
[165] Y. Liu, H. Aziguli, B. Zhang, W. Xu, W. Lu, J. Bernholc, Q. Wang, Ferroelectric polymers exhibiting behaviour reminiscent of a morphotropic phase boundary, Nature 562 (7725) (2018) 96–100.
[166] Y. Liu, B. Zhang, W. Xu, A. Haibibu, Z. Han, W. Lu, J. Bernholc, Q. Wang, Chirality-induced relaxor properties in ferroelectric polymers, Nat. Mater. 19 (11) (2020) 1169–1174.
[167] C.K. Jeong, K.-I. Park, J.H. Son, G.-T. Hwang, S.H. Lee, D.Y. Park, H.E. Lee, H. K. Lee, M. Byun, K.J. Lee, Self-powered fully-flexible light-emitting system enabled by flexible energy harvester, Energy Environ. Sci. 7 (12) (2014) 4035–4043.
[168] J. Park, Y.-w. Lim, S.Y. Cho, M. Byun, K.-I. Park, H.E. Lee, S.D. Bu, K.-T. Lee, Q. Wang, C.K. Jeong, Ferroelectric polymer nanofibers reminiscent of morphotropic phase boundary behavior for improved piezoelectric energy harvesting, Small 18 (15) (2022), 2104472.
[169] G. Zhang, P. Zhao, X. Zhang, K. Han, T. Zhao, Y. Zhang, C.K. Jeong, S. Jiang, S. Zhang, Q. Wang, Flexible three-dimensional interconnected piezoelectric ceramic foam based composites for highly efficient concurrent mechanical and thermal energy harvesting, Energy Environ. Sci. 11 (8) (2018) 2046–2056.
[170] H. Liu, J. Geng, Q. Zhu, L. Zhang, F. Wang, T. Chen, L. Sun, Flexible ultrasonic transducer array with bulk PZT for adjuvant treatment of bone injury, Sensors 20 (1) (2019).
[171] P. Jin, J. Fu, F. Wang, Y. Zhang, P. Wang, X. Liu, Y. Jiao, H. Li, Y. Chen, Y. Ma, X. Feng, A flexible, stretchable system for simultaneous acoustic energy transfer and communication, Sci. Adv. 7 (40) (2021), eabg2507.
[172] A.S. Dahiya, F. Morini, S. Boubenia, K. Nadaud, D. Alquier, G. Poulin-Vittrant, Organic/inorganic hybrid stretchable piezoelectric nanogenerators for self-powered wearable electronics, Adv. Mater. Technol 3 (2) (2018), 1700249.
[173] S.-H. Shin, Y.-H. Kim, M.H. Lee, J.-Y. Jung, J.H. Seol, J. Nah, Lithium-doped zinc oxide nanowires–polymer composite for high performance flexible piezoelectric nanogenerator, ACS Nano 8 (10) (2014) 10844–10850.
[174] T. Charoonsuk, S. Sriphan, C. Nawanil, N. Chanlek, W. Vittayakorn, N. Vittayakorn, Tetragonal BaTiO3 nanowires: a template-free salt-flux-assisted synthesis and its piezoelectric response based on mechanical energy harvesting, J. Mater. Chem. C 7 (27) (2019) 8277–8286.
[175] K.-I. Park, M. Lee, Y. Liu, S. Moon, G.-T. Hwang, G. Zhu, J.E. Kim, S.O. Kim, D. K. Kim, Z.L. Wang, K.J. Lee, Flexible nanocomposite generator made of BaTiO3 nanoparticles and graphitic carbons, Adv. Mater. 24 (22) (2012) 2999–3004.
[176] Z. Wang, Q.T. Xue, Y.Q. Chen, Y. Shu, H. Tian, Y. Yang, D. Xie, J.W. Luo, T.L. Ren, A flexible ultrasound transducer array with micro-machined bulk PZT, Sensors 15 (2) (2015) 2538–2547.
[177] N.K. James, U. Lafont, S. van der Zwaag, W.A. Groen, Piezoelectric and mechanical properties of fatigue resistant, self-healing PZT–ionomer composites, Smart Mater. Struct. 23 (5) (2014).
[178] M. Yang, J. Liu, D. Liu, J. Jiao, N. Cui, S. Liu, Q. Xu, L. Gu, Y. Qin, A fully self-healing piezoelectric nanogenerator for self-powered pressure sensing electronic skin, Research 2021 (2021), 9793458.
[179] S. Bhunia, S. Chandel, S.K. Karan, S. Dey, A. Tiwari, S. Das, N. Kumar, R. Chowdhury, S. Mondal, I. Ghosh, A. Mondal, B.B. Khatua, N. Ghosh, C. M. Reddy, Autonomous self-repair in piezoelectric molecular crystals, Science 373 (6552) (2021) 321–327.
[180] S.M. Mirabedini, F. Alizadegan, Ionomers as Self-Healing Materials, Self-Healing Polymer-Based Systems, 2020, pp. 279–291.
[181] S.v.d. Zwaag, Self Healing Materials: an Alternative Approach to 20 Centuries of Materials Science, Springer, Dordrecht, 2007.
[182] M. Pan, C. Yuan, T. Pickford, J. Tian, C. Ellingford, N. Zhou, C. Bowen, C. Wan, Piezoelectric-driven self-sensing leaf-mimic actuator enabled by integration of a self-healing dielectric elastomer and a piezoelectric composite, Advanced Intelligent Systems 3 (8) (2021).
[183] X. Wang, Q. Liu, X. Hu, M. You, Q. Zhang, K. Hu, Q. Zhang, Y. Xiang, Highly stretchable lactate-based piezoelectric elastomer with high current density and fast self-healing behaviors, Nano Energy 97 (2022).
[184] F.-R. Fan, Z.-Q. Tian, Z. Lin Wang, Flexible triboelectric generator, Nano Energy 1 (2) (2012) 328–334.
[185] J. Luo, W. Gao, Z.L. Wang, The triboelectric nanogenerator as an innovative technology toward intelligent sports, Adv. Mater. 33 (17) (2021), 2004178.
[186] X.-L. Shi, J. Zou, Z.-G. Chen, Advanced thermoelectric design: from materials and structures to devices, Chem. Rev. 120 (15) (2020) 7399–7515.
[187] M. Hong, Y. Wang, W. Liu, S. Matsumura, H. Wang, J. Zou, Z.-G. Chen, Arrays of planar vacancies in superior thermoelectric Ge1−x−yCdxBiyTe with band convergence, Adv. Energy Mater. 8 (30) (2018), 1801837.
[188] M. Hong, Y. Wang, T. Feng, Q. Sun, S. Xu, S. Matsumura, S.T. Pantelides, J. Zou, Z.-G. Chen, Strong phonon–phonon interactions securing extraordinary thermoelectric Ge1−xSbxTe with Zn-Alloying-Induced band Alignment, J. Am. Chem. Soc. 141 (4) (2019) 1742–1748.
[189] Y. Yang, J.H. Jung, B.K. Yun, F. Zhang, K.C. Pradel, W. Guo, Z.L. Wang, Flexible pyroelectric nanogenerators using a composite structure of lead-free KNbO3 nanowires, Adv. Mater. 24 (39) (2012) 5357–5362.
[190] R.E. Newnham, D.P. Skinner, L.E. Cross, Connectivity and piezoelectric-pyroelectric composites, Mater. Res. Bull. 13 (5) (1978) 525–536.
[191] S. Wang, P. Chen, Y. Bai, J.-H. Yun, G. Liu, L. Wang, New BiVO4 dual photoanodes with enriched oxygen vacancies for efficient solar-driven water splitting, Adv. Mater. 30 (20) (2018), 1800486.
[192] E.J. Yoo, M. Lyu, J.-H. Yun, C.J. Kang, Y.J. Choi, L. Wang, Resistive switching behavior in organic–inorganic hybrid CH3NH3PbI3−xClx perovskite for resistive random access memory devices, Adv. Mater. 27 (40) (2015) 6170–6175.
[193] Y. Bai, H. Yu, Z. Li, R. Amal, G.Q. Lu, L. Wang, In situ growth of a ZnO nanowire network within a TiO2 nanoparticle film for enhanced dye-sensitized solar cell performance, Adv. Mater. 24 (43) (2012) 5850–5856.
[194] D.W. Kim, J.H. Lee, J.K. Kim, U. Jeong, Material aspects of triboelectric energy generation and sensors, NPG Asia Mater. 12 (1) (2020).
[195] J. Zhang, Y. He, C. Boyer, K. Kalantar-Zadeh, S. Peng, D. Chu, C.H. Wang, Recent developments of hybrid piezo–triboelectric nanogenerators for flexible sensors and energy harvesters, Nanoscale Adv. 3 (19) (2021) 5465–5486.
[196] H. Zou, Y. Zhang, L. Guo, P. Wang, X. He, G. Dai, H. Zheng, C. Chen, A.C. Wang, C. Xu, Z.L. Wang, Quantifying the triboelectric series, Nat. Commun. 10 (1) (2019) 1427.
[197] A.R. Chowdhury, A.M. Abdullah, I. Hussain, J. Lopez, D. Cantu, S.K. Gupta, Y. Mao, S. Danti, M.J. Uddin, Lithium doped zinc oxide based flexible piezoelectric-triboelectric hybrid nanogenerator, Nano Energy 61 (2019) 327–336.
[198] A.R. Chowdhury, J. Jaksik, I. Hussain, P. Tran, S. Danti, M.J. Uddin, Surface-modified nanostructured piezoelectric device as a cost-effective transducer for energy and biomedicine, Energy Technol. 7 (5) (2019), 1800767.
[199] W. He, Y. Qian, B.S. Lee, F. Zhang, A. Rasheed, J.E. Jung, D.J. Kang, Ultrahigh output piezoelectric and triboelectric hybrid nanogenerators based on ZnO nanoflakes/polydimethylsiloxane composite films, ACS Appl. Mater. Interfaces 10 (51) (2018) 44415–44420.
[200] W.-S. Jung, M.-G. Kang, H.G. Moon, S.-H. Baek, S.-J. Yoon, Z.-L. Wang, S.-W. Kim, C.-Y. Kang, High output piezo/triboelectric hybrid generator, Sci. Rep. 5 (1) (2015) 9309.
[201] X. Wang, B. Yang, J. Liu, Y. Zhu, C. Yang, Q. He, A flexible triboelectric-piezoelectric hybrid nanogenerator based on P(VDF-TrFE) nanofibers and PDMS/MWCNT for wearable devices, Sci. Rep. 6 (1) (2016), 36409.
[202] J. Zhu, X. Hou, X. Niu, X. Guo, J. Zhang, J. He, T. Guo, X. Chou, C. Xue, W. Zhang, The d-arched piezoelectric-triboelectric hybrid nanogenerator as a self-powered vibration sensor, Sensor Actuator Phys. 263 (2017) 317–325.
[203] X. Chen, M. Han, H. Chen, X. Cheng, Y. Song, Z. Su, Y. Jiang, H. Zhang, A wave-shaped hybrid piezoelectric and triboelectric nanogenerator based on P(VDF-TrFE) nanofibers, Nanoscale 9 (3) (2017) 1263–1270.
[204] R.W. Whatmore, Pyroelectric devices and materials, Rep. Prog. Phys. 49 (12) (1986) 1335–1386.
[205] Y. Chen, Y. Zhang, F. Yuan, F. Ding, O.G. Schmidt, A flexible PMN-PT ribbon-based piezoelectric-pyroelectric hybrid generator for human-activity energy harvesting and monitoring, Adv. Electron. Mater. 3 (3) (2017), 1600540.
[206] M.-H. You, X.-X. Wang, X. Yan, J. Zhang, W.-Z. Song, M. Yu, Z.-Y. Fan, S. Ramakrishna, Y.-Z. Long, A self-powered flexible hybrid piezoelectric–pyroelectric nanogenerator based on non-woven nanofiber membranes, J. Mater. Chem. 6 (8) (2018) 3500–3509.
[207] X. Chen, J. Shao, X. Li, H. Tian, A flexible piezoelectric-pyroelectric hybrid nanogenerator based on P(VDF-TrFE) nanowire array, IEEE Trans. Nanotechnol. 15 (2) (2016) 295–302.
[208] Y. Wang, L. Yang, X.-L. Shi, X. Shi, L. Chen, M.S. Dargusch, J. Zou, Z.-G. Chen, Flexible thermoelectric materials and generators: challenges and innovations, Adv. Mater. 31 (29) (2019), 1807916.
[209] Z.-G. Chen, G. Han, L. Yang, L. Cheng, J. Zou, Nanostructured thermoelectric materials: current research and future challenge, Prog. Nat. Sci.: Mater. Int. 22 (6) (2012) 535–549.
[210] M. Hong, Z.-G. Chen, J. Zou, Fundamental and progress of Bi_2Te_3 -based thermoelectric materials, Chin. Phys. B 27 (4) (2018), 048403.
[211] Q. Xianbo, Y. Jingqi, Temperature control for PCR thermocyclers based on peltier-effect thermoelectric, in: 2005 IEEE Engineering in Medicine and Biology 27th Annual Conference, 2005, pp. 7509–7512.
[212] Y. Wang, W.-D. Liu, X.-L. Shi, M. Hong, L.-J. Wang, M. Li, H. Wang, J. Zou, Z.-G. Chen, Enhanced thermoelectric properties of nanostructured n-type Bi_2Te_3 by suppressing Te vacancy through non-equilibrium fast reaction, Chem. Eng. J. 391 (2020), 123513.
[213] Y. Wang, W.-D. Liu, H. Gao, L.-J. Wang, M. Li, X.-L. Shi, M. Hong, H. Wang, J. Zou, Z.-G. Chen, High porosity in nanostructured n-type Bi_2Te_3 obtaining ultralow lattice thermal conductivity, ACS Appl. Mater. Interfaces 11 (34) (2019) 31237–31244.
[214] S. Kumar, H.H. Singh, N. Khare, Flexible hybrid piezoelectric-thermoelectric generator for harnessing electrical energy from mechanical and thermal energy, Energy Convers. Manag. 198 (2019), 111783.

[215] S. Lee, S.-H. Bae, L. Lin, S. Ahn, C. Park, S.-W. Kim, S.N. Cha, Y.J. Park, Z.L. Wang, Flexible hybrid cell for simultaneously harvesting thermal and mechanical energies, Nano Energy 2 (5) (2013) 817–825.
[216] S. Kim, D.Y. Hyeon, S.S. Ham, J. Youn, H.S. Lee, S. Yi, K.T. Kim, K.-I. Park, Synergetic enhancement of the energy harvesting performance in flexible hybrid generator driven by human body using thermoelectric and piezoelectric combine effects, Appl. Surf. Sci. 558 (2021).
[217] L. Zhang, X.-L. Shi, Y.-L. Yang, Z.-G. Chen, Flexible thermoelectric materials and devices: from materials to applications, Mater. Today 46 (2021) 62–108.
[218] S. Xu, X.-L. Shi, M. Dargusch, C. Di, J. Zou, Z.-G. Chen, Conducting polymer-based flexible thermoelectric materials and devices: from mechanisms to applications, Prog. Mater. Sci. 121 (2021), 100840.
[219] Y. Wang, M. Hong, W.-D. Liu, X.-L. Shi, S.-D. Xu, Q. Sun, H. Gao, S. Lu, J. Zou, Z.-G. Chen, $Bi_{0.5}Sb_{1.5}Te_3$/PEDOT:PSS-based flexible thermoelectric film and device, Chem. Eng. J. 397 (2020), 125360.
[220] Y. Oh, D.-S. Kwon, Y. Eun, W. Kim, M.-O. Kim, H.-J. Ko, S.G. Kang, J. Kim, Flexible energy harvester with piezoelectric and thermoelectric hybrid mechanisms for sustainable harvesting, International Journal of Precision Engineering and Manufacturing-Green Technology 6 (4) (2019) 691–698.
[221] M. Tan, W.-D. Liu, X.-L. Shi, H. Gao, H. Li, C. Li, X.-B. Liu, Y. Deng, Z.-G. Chen, Anisotropy control–induced unique anisotropic thermoelectric performance in the n-type Bi2Te2.7Se0.3 thin films, Small Methods 3 (11) (2019), 1900582.
[222] D.S. Montgomery, C.A. Hewitt, D.L. Carroll, Hybrid thermoelectric piezoelectric generator, Appl. Phys. Lett. 108 (26) (2016).
[223] P. Zhu, Y. Wang, M. Sheng, Y. Wang, Y. Yu, Y. Deng, A flexible active dual-parameter sensor for sensitive temperature and physiological signal monitoring via integrating thermoelectric and piezoelectric conversion, J. Mater. Chem. 7 (14) (2019) 8258–8267.
[224] D. Choi, K.Y. Lee, M.-J. Jin, S.-G. Ihn, S. Yun, X. Bulliard, W. Choi, S.Y. Lee, S.-W. Kim, J.-Y. Choi, J.M. Kim, Z.L. Wang, Control of naturally coupled piezoelectric and photovoltaic properties for multi-type energy scavengers, Energy Environ. Sci. 4 (11) (2011).
[225] C. Pan, W. Guo, L. Dong, G. Zhu, Z.L. Wang, Optical fiber-based core-shell coaxially structured hybrid cells for self-powered nanosystems, Adv. Mater. 24 (25) (2012) 3356–3361.
[226] C. Xu, Z.L. Wang, Compact hybrid cell based on a convoluted nanowire structure for harvesting solar and mechanical energy, Adv. Mater. 23 (7) (2011) 873–877.
[227] G.C. Yoon, K.-S. Shin, M.K. Gupta, K.Y. Lee, J.-H. Lee, Z.L. Wang, S.-W. Kim, High-performance hybrid cell based on an organic photovoltaic device and a direct current piezoelectric nanogenerator, Nano Energy 12 (2015) 547–555.
[228] Q. Schiermeier, J. Tollefson, T. Scully, A. Witze, O. Morton, Energy alternatives: electricity without carbon, Nature 454 (7206) (2008) 816–823.
[229] W. Feng, J.-F. Liao, X. Chang, J.-X. Zhong, M. Yang, T. Tian, Y. Tan, L. Zhao, C. Zhang, B.-X. Lei, L. Wang, J. Huang, W.-Q. Wu, Perovskite crystals redissolution strategy for affordable, reproducible, efficient and stable perovskite photovoltaics, Mater. Today 50 (2021) 199–223.
[230] W. Feng, Y. Tan, M. Yang, Y. Jiang, B.-X. Lei, L. Wang, W.-Q. Wu, Small amines bring big benefits to perovskite-based solar cells and light-emitting diodes, Chem 8 (2) (2021) 351–383.
[231] T. Tian, J.-X. Zhong, M. Yang, W. Feng, C. Zhang, W. Zhang, Y. Abdi, L. Wang, B.-X. Lei, W.-Q. Wu, Interfacial linkage and carbon encapsulation enable full solution-printed perovskite photovoltaics with prolonged lifespan, Angew. Chem. Int. Ed. 60 (44) (2021) 23735–23742.
[232] Y. Bai, M. Hao, S. Ding, P. Chen, L. Wang, Surface Chemistry engineering of perovskite quantum dots: strategies, applications, and perspectives, Adv. Mater. n/a (n/a) 2105958.
[233] S. Gong, W. Cheng, Toward soft skin-like wearable and implantable energy devices, Adv. Energy Mater. 7 (23) (2017), 1700648.
[234] X. Wu, Q. Guo, Bioresorbable photonics: materials, devices and applications, Photonics 8 (7) (2021).
[235] J. Zhao, R. Ghannam, K.O. Htet, Y. Liu, M.-k. Law, V.A.L. Roy, B. Michel, M. A. Imran, H. Heidari, Self-Powered implantable medical devices: photovoltaic energy harvesting review, Adv. Healthc. Mater. 9 (17) (2020), 2000779.
[236] B. Parida, S. Iniyan, R. Goic, A review of solar photovoltaic technologies, Renew. Sustain. Energy Rev. 15 (3) (2011) 1625–1636.
[237] X. Liu, J. Li, Z. Fang, C. Wang, L. Shu, J. Han, Ultraviolet-protecting, flexible and stable photovoltaic-assisted piezoelectric hybrid unit nanogenerator for simultaneously harvesting ultraviolet light and mechanical energies, Materials in Medicine 55 (31) (2020) 15222–15237.
[238] D. Vatansever, R.L. Hadimani, T. Shah, E. Siores, Hybrid photovoltaic-piezoelectric flexible device for energy harvesting from nature, Adv. Sci. Technol. (2013) 297–301.
[239] R. Ahmed, Y. Kim, Zeeshan, W. Chun, Development of a tree-shaped hybrid nanogenerator using flexible sheets of photovoltaic and piezoelectric films, Energies 12 (2) (2019).
[240] J. Zhou, N.S. Xu, Z.L. Wang, Dissolving behavior and stability of ZnO wires in biofluids: a study on biodegradability and biocompatibility of ZnO nanostructures, Adv. Mater. 18 (18) (2006) 2432–2435.
[241] J. Liu, P. Fei, J. Zhou, R. Tummala, Z.L. Wang, Toward high output-power nanogenerator, Appl. Phys. Lett. 92 (17) (2008), 173105.
[242] K.-H. Kim, B. Kumar, K.Y. Lee, H.-K. Park, J.-H. Lee, H.H. Lee, H. Jun, D. Lee, S.-W. Kim, Piezoelectric two-dimensional nanosheets/anionic layer heterojunction for efficient direct current power generation, Sci. Rep. 3 (1) (2013) 2017.
[243] Y. Zi, L. Lin, J. Wang, S. Wang, J. Chen, X. Fan, P.K. Yang, F. Yi, Z.L. Wang, Triboelectric-pyroelectric-piezoelectric hybrid cell for high-efficiency energy-harvesting and self-powered sensing, Adv. Mater. 27 (14) (2015) 2340–2347.
[244] K. Zhang, S. Wang, Y. Yang, A one-structure-based piezo-tribo-pyro-photoelectric effects coupled nanogenerator for simultaneously scavenging mechanical, thermal, and solar energies, Adv. Energy Mater. 7 (6) (2016).
[245] C. Zhang, H. Chen, X. Ding, F. Lorestani, C. Huang, B. Zhang, B. Zheng, J. Wang, H. Cheng, Y. Xu, Human motion-driven self-powered stretchable sensing platform based on laser-induced graphene foams, Appl. Phys. Rev. 9 (1) (2022), 011413.
[246] J. Zhu, J.J. Fox, N. Yi, H. Cheng, Structural design for stretchable microstrip antennas, ACS Appl. Mater. Interfaces 11 (9) (2019) 8867–8877.
[247] S. Zhang, J. Zhu, Y. Zhang, Z. Chen, C. Song, J. Li, N. Yi, D. Qiu, K. Guo, C. Zhang, T. Pan, Y. Lin, H. Zhou, H. Long, H. Yang, H. Cheng, Standalone stretchable RF systems based on asymmetric 3D microstrip antennas with on-body wireless communication and energy harvesting, Nano Energy 96 (2022), 107069.
[248] C. Wang, Y. Yu, Y. Yuan, C. Ren, Q. Liao, J. Wang, Z. Chai, Q. Li, Z. Li, Heartbeat-sensing mechanoluminescent device based on a quantitative relationship between pressure and emissive intensity, Matter 2 (1) (2020) 181–193.
[249] M.S. Senousy, R.K.N.D. Rajapakse, D. Mumford, M.S. Gadala, Self-heat generation in piezoelectric stack actuators used in fuel injectors, Smart Mater. Struct. 18 (4) (2009).
[250] C. Yu, G. Zhang, Y.-W. Zhang, L.-M. Peng, Strain engineering on the thermal conductivity and heat flux of thermoelectric Bi2Te3 nanofilm, Nano Energy 17 (2015) 104–110.
[251] H.S. Choi, Architectural simulation of hybrid energy harvesting: a design experiment in Lanzarote island, Appl. Sci. 11 (24) (2021), 12146.
[252] J. Brancart, G. Scheltjens, T. Muselle, B. Van Mele, H. Terryn, G. Van Assche, Atomic force microscopy–based study of self-healing coatings based on reversible polymer network systems, J. Intell. Mater. Syst. Struct. 25 (1) (2012) 40–46.
[253] M.S. Dargusch, J. Venezuela, A. Dehghan-Manshadi, S. Johnston, N. Yang, K. Mardon, C. Lau, R. Allavena, *In vivo* evaluation of bioabsorbable Fe-35Mn-1Ag: first reports on i*n vivo* hydrogen gas evolution in Fe-based implants, Adv. Healthc. Mater. 10 (2) (2021), 2000667.